Analysis of Compartments-In-Series Models of Liver Metabolism as PDEs: the Effect of Dispersion and Number of Compartments

M. Noorman[1], R. Allen[2], C.J. Musante[2], H.T. Banks[1]

[1]Center for Research in Scientific Computation
Department of Mathematics
North Carolina State University
Raleigh, NC 27695-8212

[2]Pfizer Inc.
Cambridge, MA 02139

September 26, 2018

Abstract

Non-alcoholic fatty liver disease (NAFLD) is the most common cause of chronic liver disease and can lead to cirrhosis and liver cancer. Precipitated by the build up of extra fat in the liver not caused by alcohol, it is still not understood why steatosis occurs where it does in the liver microstructure in NAFLD. It is likely, however, that the location of steatosis is due, at least in part, to metabolic zonation (heterogeneity among liver cells in function and enzyme expression). Recently, there has been an influx of computational and mathematical models in order to investigate the relationship between metabolic zonation and steatosis in NAFLD. Of interest among these models are "comparments-in-series" models. These compartmental models include the spatial distribution of metabolite concentrations via series of compartments that are connected through some representation of blood flow. In this paper, we will analyze one such model, looking at how the number of compartments as well as inclusion of dispersion in the flow affect simulation results.

1 Introduction

Non-alcholic fatty liver disease (NAFLD) encompasses a spectrum of liver disease that begins as noninflammatory build-up of extra fat in liver cells (steatosis), can progress to non-alcoholic steatohepatitis (NASH) which is the occurrence of inflammation and liver damage in addition to the steatosis and eventually lead to cirrhosis [5, 8, 41]. Globally, an estimated 11-46% of people suffer from NAFLD [5, 8, 37]. Approximately 25-40% of patients with NAFLD will progress to NASH [8] with 40-50% of patients developing fibrosis and 20% developing cirrhosis [6]. The increasing prevalence of NAFLD has been linked to the rise of obesity [6] and is strongly associated with insulin resistance and type 2 diabetes mellitus [6, 8, 37, 41]. Considered the hepatic manifestation of metabolic syndrome [8, 15, 41], NAFLD is currently the most common cause of chronic liver disease [5, 8] and NASH is the second leading cause of cirrhosis in adults waiting for liver transplants in the United States [5, 37, 39], expected to become the first leading cause by

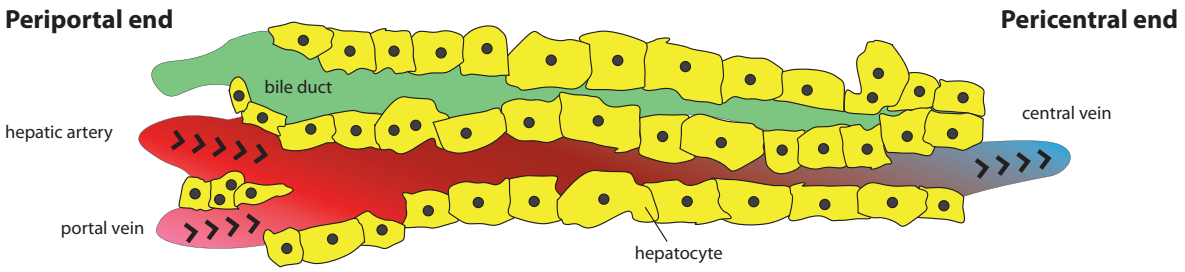

Figure 1: Portal axis of a liver sinusoid.

2030 [5, 6]. It has also been suggested that a recent increase in the prevalence of hepatocellular carcinoma is caused by NAFLD [5, 80].

As the prevalence of NAFLD continues to increase, the cause and pathogenesis of the disease remains an area of intensive study. Though our understanding of this disease has progressed substantially and continues to grow, there is much still to uncover. The pathogenesis of NAFLD is multifactorial and extremely complex, comprised of environmental and genetic factors, the specific contributions of which are not yet known [5]. Further, though the metabolic processes involved in steatosis have been investigated for decades, there is still much unknown about why lipids accumulate where they do in the liver.

In the continuing investigation of this disease, mathematical and computational models will serve an important role as they give us the ability to explore the complex relationships between various components in a low cost setting. In this paper, we will look at a model of the liver metabolism and examine certain aspects of it in order to inform future development of such models.

1.1 Relevant Biology

The liver is the main metabolic organ in the human body and, as such, plays a central role in the regulation of key metabolites including glucose and free fatty acid (FFA). Most of the metabolic processes that occur in the liver take place in the hepatocyte, the main cell type of the liver. These hepatocytes are tightly organized into tesselating columns embedded into liver lobules which make up each of the four lobes of the liver. The lobules have hexagonal cross sections, each corner of which harbors a portal triad which is comprised of a bile duct, hepatic artery (which supplies the hepatocytes with oxygenated blood), and a portal vein (which supplies the hepatocytes with nutrient filled blood). The blood exits the lobule through the central vein which is located at the center of the hexagonal structures. Numerous capillaries, called sinusoids, connect the periportal blood vessels of the portal triad with the central vein (see Figure 1). These sinusoids are surrounded by the columns of hepatocytes and are the mechanism through which the hepatocytes have access to the blood provided by the portal triad.

Hepatocytes vary in enzyme expression and function depending upon where they lie along the sinusoid, a phenomena called zonation [36, 44, 45, 46, 49, 50, 51]. This heterogeneity among hepatocytes is, at least in part, the result of differing concentrations of metabolites and signaling molecules along the sinusoid. For example, as blood flows through the sinusoid, oxygen diffuses and is taken up into the hepatocytes resulting in higher levels of oxygen on the periportal end

of the sinusoid (near the portal triad) and lower levels of oxygen on the pericentral end of the sinusoid (near the central vein). This oxygen gradient was discovered decades ago and has long since been considered a significant driving force of zonation [12, 47, 48, 52, 53, 54, 81]. Some studies have also indicated that the hormones insulin and glucagon play an important role in the regulation of zonated gene expression [46, 49, 66]. More recently, other signaling pathways have also been proposed and studied as potential mechanisms for zonation [23, 42, 79].

Metabolic zonation is not the only form of heterogeneity seen across the sinusoid. Most liver diseases show a varying amount of damage across the liver microstructure [46]. In NAFLD, studies have shown that, for adult patients, steatosis is typically most severe in pericentral cells [2, 16, 17, 21, 42, 83]. However not all patients show such an aberrant accumulation of lipids on a particular part of the sinusoid [17, 21]. Further, steatosis in pediatric patients with NAFLD tends to occur most severely in periportal cells [83]. The cause of this "zonated steatosis" in NAFLD is still not fully understood, however the heterogeneity of hepatocytes likely results in certain liver cells being more vulnerable to lipid build up than others [7]. Further, in patients who have progressed to NASH, inflammation and fibrosis tends to be most severe on the pericentral end of the sinusoid [1, 16, 21, 42].

Although it is well known that lipids tend to accumulate heterogeneously across the sinusoid (both in NAFLD and in other liver diseases), the effect of metabolic zonation on such zonated steatosis has received limited attention experimentally. To great extent, this is because investigating changes in individual regions of the sinusoid is extremely time consuming and complex [7]. Computational models of liver metabolism that are spatially distributed give us the ability to explore relationships between metabolic zonation and zonated steatosis without the high cost of experimentation. Since NAFLD is induced by a change in metabolism, that is, the build up of lipids in the liver, it is tangible that metabolic zonation plays a major role in the pathology of this disease. Thus, the development of computational models of liver metabolism that include the spatial effects of zonation are of utmost importance in the continuing effort to understand and find treatment for NAFLD.

1.2 Spatially Distributed Models of Liver Metabolism

Computational models have been used previously to study the effect of zonation on detoxification processes such as the detoxification of ammonia [62], xenobiotics [75], and drugs [64, 68], as well as more generally in pharmacokinetics [4, 63]. However, few models currently exist that explicitly consider the heterogeneous expression of enzymes which defines metabolic zonation.

Existing mechanistic models of liver metabolism that include spatial distribution can be roughly divided into two categories depending on the types of equations used: those which use partial differential equations (PDEs) and those which use ordinary differential equations (ODEs). As will be shown later on, models from different categories may not always be as different from each other as may appear at first glance. The PDE models can further be divided into models derived using the theory of porous media and models that utilize advection or advection-dispersion equations.

The advantages of deriving a system using the theory of porous media is in the ability to more accurately describe the process of blood perfusion through the liver lobule. This is of particular interest since steatosis can affect hepatic hemodynamics [31, 56, 60, 77]. In a series of publications [69, 70, 71], Ricken et al. develop a multi scale approach that does just this, coupling the blood

perfusion through the liver lobule with a description of hepatic cell metabolism. While metabolic zonation is not explicitly included, they are still able to simulate some zonated steatosis.

Models using advection or advection-dispersion equations to represent the blood flow in the liver have been around for decades finding applications in many areas such as hepatic elimination, drug clearance, and capillary tissue exchange [9, 10, 27, 63, 72]. These models have generally been referred to as parallel-tube and distributed models (advective flow) [9, 10, 34] and dispersion models (advective-dispersive flow) [73]. Similar models to the dispersion model have been used in the past decade to study aspects of hepatic metabolism as well [19, 22]. In 2006, Chalhoub et al. [22] used advection-dispersion-reaction equations to represent the concentrations of metabolites in the sinusoid, coupled through metabolic transport to mass-balance equations for the metabolites in the tissue. Enzymatic zonation is included for central carbohydrate pathways, but not for lipid metabolism. In 2008, Calvetti et al. [19] used a model similar to the one given in [22] to illustrate how one may embed such a model of cellular liver metabolism into a Bayesian framework for parameter estimation purposes. However, zonation is excluded from the model and the system is only considered at steady state. Use of these types of PDEs to model the liver microstructure has appeared to lag in the past decade as compartmental models have started to show prevalence. An explanation for this may be due to the appearance of these PDEs as being more difficult to use in comparison to compartmental models which are composed of ODEs [4, 38].

Compartmental models for the liver that include spatial distribution were originally inspired by "tanks-in-series" models from chemical engineering [38] and can be considered "compartments-in-series" models. These models are comprised of systems of ODEs derived by considering a series of compartments that are connected together, typically through blood flow. While early models of this type had each compartment represent both blood and tissue [38] so that there is only a single series of compartments, modern models tend to separate blood and tissue into different compartments with a transport between them [6, 7, 11, 62, 74]. These models have a series of hepatic blood compartments that are connected through blood flow along with a series of tissue compartments which are only connected to their corresponding hepatic blood compartment (i.e., there is no explicit connection between tissue compartments). These models often treat the series of compartments as being lined up along the portocentral axis of the liver sinusoid, and as such treat this as the repeating unit of the liver (rather than the hepatocyte). Recently, compartmental models that include spatial distribution have been applied more specifically to hepatic metabolism.

Schleicher et al. [74] used a three compartment model to simulate hepatic lipid metabolism. The hepatic blood flow is a basic advective flow that transports concentrations of metabolites in the hepatic blood from the periportal to the pericentral end of the sinusoid. This three compartment model is used to look at how the plasma oxygen gradient, plasma FA gradient, as well as the process for FA uptake affect the zonation of steatosis under a high-fat diet. Despite the fact that zonated enzyme expressions are not included in this model, model simulations do show a zonated steatosis.

A much more complex compartmental model was used by Berndt et al. [11] to study glucose metabolism and how it is affected by zonated enzyme expressions, metabolite and hormone gradients in the sinusoid, and blood perfusion. This model includes the blood in the sinusoid, accompanying space of Disse, as well as the adjacent layers of hepatocytes allowing the authors to take into account both morphological and systemic parameters. Each component (sinusoid,

space of Disse, and hepatocytes) is partitioned into $20-25$ compartments and flow is modeled in both the sinusoid and the space of Disse as an advective-dispersive flow.

Among the most advanced compartmental models for liver metabolism is the one presented by Ashworth et al. in [6, 7]. This 8 compartment model does not include any morphology like the model in [11], however it does include a rather detailed representation of glucose, lipid, and energy metabolism including zonated enzyme expressions and metabolite and hormone gradients in the hepatic blood. The blood flow through the sinusoid is given by a simple advective flow from the periportal to the pericentral end of the sinusoid. This model was used to investigate causes of pericentral cell susceptibility to steatosis in NAFLD, especially in the case of insulin resistance. A distinctive aspect of this model is the inclusion of an extra compartment that holds a simplified representation of metabolism in the rest of the body including hormone release by the pancreas. This extra "body" compartment acts as an input into the first hepatic blood compartment of the series of compartments and takes the output of the final hepatic blood compartment to update its own concentrations, thus creating a type of feedback into the system.

As NAFLD becomes more and more prevalent, the ability to perform accurate *in silico* experiments is an integral part of uncovering important mechanisms and targets for these conditions. Compartments in series models are an attractive tool that allow one to investigate how metabolic zonation, hepatic blood gradients of metabolites and hormones, and even blood perfusion, affect liver metabolism at various levels of complexity. In particular, these models boast the ability to investigate various aspects of liver metabolism with sharp detail while keeping computational times reasonable. However, one may question if the simplification to a number of compartments rather than a continuum may result in the loss of information or misrepresentation of results. In what follows, we will examine a model similar to the one presented in [6, 7] in order to begin attempting to answer this question. The two main goals of this paper are (i) to investigate the effect that the number of compartments has on model simulations and (ii) to investigate the effect of dispersion on the system.

2 The Model

We present here the models of the liver microstructure under consideration. Our models closely resembles that of [6, 7], with the main differences being how concentrations in the systemic blood are modeled as well as how we view the equations in the hepatic blood.

We model the concentrations of a number of metabolites, hormones, and oxygen in the liver sinusoid. Equations are separated into those for the hepatocytes (referred to as hepatic equations), for hepatic blood (i.e., blood/plasma in the sinusoid), and systemic blood (i.e., blood/plasma in the rest of the body). While oxygen, hormones, and metabolites are all modeled in the hepatic and systemic blood, only metabolites are modeled in the hepatocyte. However, the concentration of hormones and oxygen in the hepatic blood do affect the metabolic processes that occur in the hepatocyte. A full list of all the concentrations modeled is included in Table 1 along with what kinds of equations they have and their abbreviated variable name that will be used to denote them throughout this paper. Figure 2 gives a schematic of the overall structure of the model. We will use the following notation convention: variables in the hepatocyte will have a subscript H, variables in the hepatic blood will have a subscript HB, and variables in the systemic blood will have a subscript SB. The only exception to this will be molecules whose concentrations are only modeled in the hepatocyte (see the third column of Table 1) which will not have any subscript.

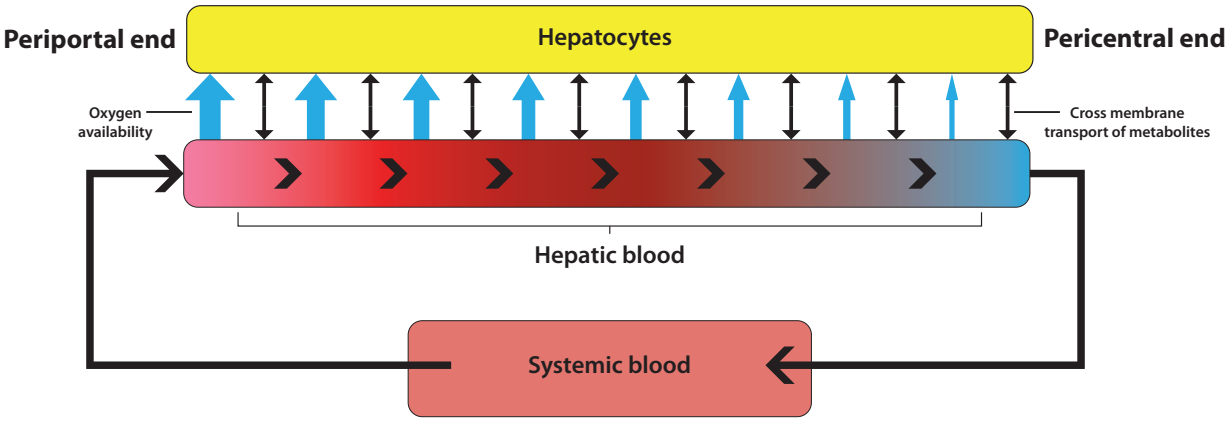

Figure 2: Schematic of PDE model.

Equations in H, HB, SB		Equations in HB, SB		Equations in H	
Glucose	gC	Insulin	Ins	Glycogen	G
Triglycerides	TG	Glucagon	GL	Glucose-6-phosphate	$g6p$
Fatty acids	FA	Oxygen	Oxy	Glycerol-3-phosphate	$g3p$
Glycerol	gly			Acetyl-CoA	$aCoA$
Lactate	Lac			Inorganic phosphate	P
				Guanosine Tri/Di-phosphate	gtp/gdp
				Uridine Tri/Di-phosphate	utp/udp
				Adenosine Tri/Di/Mono-phosphate	$atp/adp/amp$

Table 1: All molecules represented in the model with their abbreviated variable name. H denotes hepatic, HB denotes hepatic blood, SB denotes systemic blood.

2.1 Hepatocytes

The equations for molecule concentrations in the hepatocytes are given in Table 3 below.

In the model presented in [6, 7], the rate of hepatic metabolic processes are modeled through the use of Hill functions. Rather than modeling every individual enzyme, sections of the metabolic pathways are often modeled by a single function, thus depending upon a number of intermediate enzymes rather than a single one. Each substrate and allosteric activator/inhibitor is represented by a Hill function and the rate of the process is calculated to be the product of these Hill functions. The hepatic metabolic processes included in the model are given in Table 4 along with the function for the rate of that process.

The transport of metabolites between plasma and hepatocyte are modeled similarly. For uni-directional transports, the rate is calculated using a Hill function where the plasma molecule is treated as the substrate and the hepatic molecule as the product. For bi-directional transports, the rate is calculated by a "Hill-like" function that depends on the difference in concentration of the molecule between the plasma and hepatocyte. Table 2 shows the rates of transport of metabolites between plasma and hepatocyte.

The regulation of fatty acid (FA) transport and uptake into the liver is a complex and often

Transport	Rate
Glycerol	$\mathcal{T}_{gly} = \frac{v^{gly}([gly_{HB}]-[gly_H])}{K_M^{gly}+[gly_{HB}]+[gly_H]}$
Triglyceride	$\mathcal{T}_{TG} = -\frac{v^{VLDL}[TG_H]}{K_M^{VLDL}+[TG_H]} + \frac{v^{TG}\left([TG_{HB}]-\frac{[TG_H]}{TG_{ref}}\right)}{K_M^{TG}+[TG_{HB}]+\frac{[TG_H]}{TG_{ref}}}$
Fatty acid	$\mathcal{T}_{FA} = \frac{v^{FA}([FA_{HB}]-[FA_H]}{K_M^{FA}+[FA_{HB}]+[FA_H]}$
Glucose (GLUT2)	$\mathcal{T}_{gC} = \frac{v^{gC_{pump}}[gC_{HB}]}{K_M^{gC_{pump}}+[gC_{HB}]} + \frac{v^{gC_{diff}}([gC_{HB}]-[gC_H])}{K_M^{gC_{diff}}+[gC_{HB}]+[gC_H]}$
Lactate	$\mathcal{T}_{Lac} = \frac{v^{Lac}([Lac_{HB}]-[Lac_H])}{K_M^{Lac}+[Lac_{HB}]+[Lac_H]}$

Table 2: Transports between hepatocytes (H) and hepatic blood (HB).

debated topic [57]. There is strong evidence for protein-mediated FA uptake with a number of membrane proteins being implicated [3, 57]. In particular, in the liver such proteins include fatty acid translocase FAT/CD36 [18, 57, 58], liver fatty acid binding protein LFABP [61, 67], and fatty acid transport proteins, specifically FATP2, FATP3, and FATP5 [3, 13, 14, 29, 30, 32, 57, 59]. Passive diffusion also contributes to hepatic FA uptake, however this process is minimal in comparison to facilitated uptake [57].

In [6, 7], the FFA transport is composed of a uni-directional, insulin dependent term and a bi-directional, insulin independent term. We omit the insulin dependent term here as, under physiological conditions, the hepatic FA transporters that appear to be the major players in hepatic FA uptake (LFABP, FATP2, FATP3, and FATP5) [3, 14, 61] are not known to be regulated by insulin. The greatest evidence for insulin regulated hepatic FA uptake is in FAT/CD36 mediated FA uptake.

FAT/CD36 is a fatty acid transporter that is regulated by muscle contraction and/or insulin and is an important protein implicated in FA uptake by skeletal muscle cells, cardiomyocytes, and adipocytes [18]. Under physiological conditions, FAT/CD36 is weakly expressed in hepatocytes suggesting FA uptake is largely FAT/CD36 independent [18]. However, there is evidence that hepatic mRNA and protein levels of FAT/CD36 at the plasma membrane of hepatocytes increases in patients with NAFLD [18, 57, 58].

Of the FATP family of transporters, the only one known to be regulated by insulin is FATP1 [3]. While FATP1 does have some expression in the liver, this transport is more significant for skeletal muscle, heart, and adipose tissue [3, 14]. In fact, studies have shown that while mice lacking FATP1 show a decrease in insulin-stimulated long chain FA uptake in adipocytes and skeletal muscle, they actually have an increase in long chain FA uptake in the liver [82].

2.1.1 Zonation

The zonation of the enzyme expressions are modeled through the metabolic processes (pathways) they are involved in by utilizing information about the enzymes involved in the process as well as the location of the hepatocyte along the sinusoid. Hepatocytes are assigned values $z_x \in [-1, 1]$ (roughly) depending upon the concentration of oxygen in the plasma at the same point as the hepatocyte along the sinusoid. A negative z_x value indicates the hepatocyte is on the pericentral

end of the sinusoid, while a positive z_x value indicates the hepatocyte is on the periportal end.

Each metabolic process M is also assigned a zonation constant $k_M \in (-1, 1)$ that depends upon the experimentally measured ratio of the enzyme expression in periportal cells to pericentral cells. The rate constant for the metabolic process in a hepatocyte at point x along the sinusoid is then calculated as

$$v_x^M = (1 + z_x k_M) v_b^M \tag{1}$$

where v_b^M is the base-value for the rate constant of metabolic process M.

Molecule	**Equation**
Glycogen	$\frac{\partial[G]}{\partial t} = \mathcal{R}_{GS} - \mathcal{R}_{GP}$
Glucose-6-phosphate	$\frac{\partial[g6p]}{\partial t} = \mathcal{R}_{GK} - \mathcal{R}_{G6Pase} - \mathcal{R}_{GS} + \mathcal{R}_{GP} + \frac{1}{2}\mathcal{R}_{FBP} - \mathcal{R}_{PFK}$
Glucose	$\frac{\partial[gC_H]}{\partial t} = -\mathcal{R}_{GK} + \mathcal{R}_{G6Pase} + \mathcal{T}_{gC}$
Glycerol-3-phosphate	$\frac{\partial[g3p]}{\partial t} = \mathcal{R}_{PEPCK} - \mathcal{R}_{FBP} + 2\mathcal{R}_{PFK} - \mathcal{R}_{PK} - \mathcal{R}_{TSyn} + \mathcal{R}_{GlyK}$
Lactate	$\frac{\partial[Lac_H]}{\partial t} = -\mathcal{R}_{PEPCK} + \mathcal{R}_{PK} - \mathcal{R}_{PDH} + \mathcal{T}_{Lac}$
Acetyl-CoA	$\frac{\partial[aCoA]}{\partial t} = \mathcal{R}_{PDH} + 8\mathcal{R}_{\beta oxi} - \mathcal{R}_{Lgen} - \frac{1}{12}\mathcal{R}_{ATPS}$
Fatty acid	$\frac{\partial[FA_H]}{\partial t} = -\mathcal{R}_{\beta oxi} + \frac{1}{8}\mathcal{R}_{Lgen} + 3\mathcal{R}_{Lip} - 3\mathcal{R}_{TSyn} + \frac{1}{2}\mathcal{T}_{FA}$
Triglyceride	$\frac{\partial[TG_H]}{\partial t} = -\mathcal{R}_{Lip} + \mathcal{R}_{TSyn} + \mathcal{T}_{TG}$
Glycerol	$\frac{\partial[gly_H]}{\partial t} = \mathcal{R}_{Lip} - \mathcal{R}_{GlyK} + \mathcal{T}_{gly}$
Guanosine Tri-phosphate	$\frac{\partial[gtp]}{\partial t} = -\mathcal{R}_{PEPCK} + \mathcal{R}_{NDKG}$
Guanosine Di-phosphate	$\frac{\partial[gdp]}{\partial t} = \mathcal{R}_{PEPCK} - \mathcal{R}_{NDKG}$
Uridine Tri-phosphate	$\frac{\partial[utp]}{\partial t} = -\mathcal{R}_{GS} + \mathcal{R}_{NDKU}$
Uridine Di-phosphate	$\frac{\partial[udp]}{\partial t} = \mathcal{R}_{GS} - \mathcal{R}_{NDKU}$
Inorganic phosphate	$\frac{\partial[P]}{\partial t} = \mathcal{R}_{G6Pase} + 2\mathcal{R}_{GS} - \mathcal{R}_{GP} + 2\mathcal{R}_{PEPCK} + \frac{1}{2}\mathcal{R}_{FBP} - 2.25\mathcal{R}_{PK} - 2.5\mathcal{R}_{PDH} + 3\mathcal{R}_{\beta oxi} + \frac{7}{8}\mathcal{R}_{Lgen} + 7\mathcal{R}_{TSyn} - \mathcal{R}_{ATPS} + \mathcal{R}_{ATPu} - \mathcal{R}_{PReg}$
Adenosine Tri-phosphate	$\frac{\partial[atp]}{\partial t} = -\mathcal{R}_{GK} - 2\mathcal{R}_{PEPCK} - \mathcal{R}_{PFK} + 3.25\mathcal{R}_{PK} + 2.5\mathcal{R}_{PDH} - 2\mathcal{R}_{\beta oxi} - \frac{7}{8}\mathcal{R}_{Lgen} - 3\mathcal{R}_{TSyn} - \mathcal{R}_{GlyK} + \mathcal{R}_{ATPS} - \mathcal{R}_{NDKU} - \mathcal{R}_{NDKG} - \mathcal{R}_{AK} - \mathcal{R}_{ATPu}$
Adenosine Di-phosphate	$\frac{\partial[adp]}{\partial t} = \mathcal{R}_{GK} + 2\mathcal{R}_{PEPCK} + \mathcal{R}_{PFK} - 3.25\mathcal{R}_{PK} - 2.5\mathcal{R}_{PDH} + \mathcal{R}_{\beta oxi} + \frac{7}{8}\mathcal{R}_{Lgen} + \mathcal{R}_{GlyK} - \mathcal{R}_{ATPS} + \mathcal{R}_{NDKU} + \mathcal{R}_{NDKG} + 2\mathcal{R}_{AK} + \mathcal{R}_{ATPu}$
Adenosine Mono-phosphate	$\frac{\partial[amp]}{\partial t} = \mathcal{R}_{\beta oxi} + 3\mathcal{R}_{TSyn} - \mathcal{R}_{AK}$

Table 3: Equations for hepatic concentrations (H).

Metabolic process	Abbreviation	Rate
Glucokinase	GK	$\mathcal{R}_{GK} = v_x^{GK}\left(\frac{[gC_H]^{n_{GK}^{act}}}{(K_{GK}^{act})^{n_{GK}^{act}}+[gC_H]^{n_{GK}^{act}}}\right)\left(\frac{[gC_H]^{n_{GK}^{gC}}}{(K_{GK}^{gC})^{n_{GK}^{gC}}+[gC_H]^{n_{GK}^{gC}}}\right)\left(\frac{[atp]}{K_{GK}^{atp}+[atp]}\right)\left(1-\frac{[g6p]^{n_{GK}^{inh}}}{(K_{GK}^{inh})^{n_{GK}^{inh}}+[g6p]^{n_{GK}^{inh}}}\right)$
Glucose-6-phosphatase	$G6Pase$	$\mathcal{R}_{G6Pase} = v_x^{G6Pase}\left(\frac{[g6p]}{K_{G6Pase}^{g6p}+[g6p]}\right)$
Glycogen Synthase	GS	$\mathcal{R}_{GS} = v_x^{GS}\left(\frac{v_x^{Ins}[Ins_{HB}]+K_I^{GS}}{v_x^L[GL_{HB}]+K_L^{GS}}\right)\left(\frac{[g6p]^{nGS}}{(K_{GS}^{g6p})^{nGS}+[g6p]^{nGS}}\right)\left(\frac{[utp]}{K_{GS}^{utp}+[utp]}\right)$
Glycogen Phosphorylase	GP	$\mathcal{R}_{GP} = v^{GP}\left(\frac{v_x^L[GL_{HB}]+K_L^{GP}}{v_x^{Ins}[Ins_{HB}]+K_I^{GP}}\right)\left(\frac{[G]^{nGP}}{(K_{GP}^{G})^{nGP}+[G]^{nGP}}\right)\left(\frac{[P]}{K_{GP}^{P}+[P]}\right)$
Phosphoenolpyruvate Carboxykinase	$PEPCK$	$\mathcal{R}_{PEPCK} = v_x^{PEPCK}\left(\frac{v_x^L[GL_{HB}]+K_L^{PEPCK}}{v_x^{Ins}[Ins_{HB}]+K_I^{PEPCK}}\right)\left(\frac{[Lac_{HB}]}{K_{PEPCK}^{Lac}+[Lac_{HB}]}\right)\left(\frac{[atp]}{K_{PEPCK}^{atp}+[atp]}\right)\left(\frac{[gtp]}{K_{PEPCK}^{gtp}+[gtp]}\right)$
Fructose Biphosphatase	FBP	$\mathcal{R}_{FBP} = v_x^{FBP}\left(\frac{v_x^L[GL_{HB}]+K_L^{FBP}}{v_x^{Ins}[Ins_{HB}]+K_I^{FBP}}\right)\left(\frac{[g3p]}{K_{FBP}^{g3p}+[g3p]}\right)$
Phosphofructokinase	PFK	$\mathcal{R}_{PFK} = v^{PFK}\left(\frac{v_x^{Ins}[Ins_{HB}]+K_I^{PFK}}{v_x^L[GL_{HB}]+K_L^{PFK}}\right)\left(\frac{[g6p]}{K_{PFK}^{g6p}+[g6p]}\right)\left(\frac{[atp]}{K_{PFK}^{atp}+[atp]}\right)\left(\frac{[adp]}{K_{PFK}^{adp}+[adp]}\right)\left(1-\beta_{PFK}^{atp}\frac{[atp]}{K_{PFK}^{inh1}+[atp]}\right)\left(1-\beta_{PFK}^{g3p}\frac{[g3p]}{K_{PFK}^{inh2}+[g3p]}\right)$
Pyruvate Kinase	PK	$\mathcal{R}_{PK} = v_x^{PK}\left(\frac{v_x^{Ins}[Ins_{HB}]+K_I^{PK}}{v_x^L[GL_{HB}]+K_L^{PK}}\right)\left(\frac{[g3p]}{K_{PK}^{g3p}+[g3p]}\right)\left(\frac{[adp]}{K_{PK}^{adp}+[adp]}\right)\left(1-\beta_{PK}^{aCoA}\frac{[aCoA]}{K_{PK}^{aCoA}+[aCoA]}\right)$
Pyruvate Oxidation	PDH	$\mathcal{R}_{PDH} = v^{PDH}\left(1+v_x^{Ins}\frac{[Ins_{HB}]}{Ins_{ref}^{PDH}}-v_x^L\frac{[GL_{HB}]}{L_{ref}^{PDH}}\right)\left(\frac{[Lac_H]}{K_{PDH}^{Lac}+[Lac_H]}\right)\left(1-\frac{[aCoA]}{K_{PDH}^{aCoA}+[aCoA]}\right)$
β-Oxidation	βoxi	$\mathcal{R}_{\beta oxi} = v_x^{\beta oxi}\left(1-v_x^{Ins}\frac{[Ins_{HB}]}{Ins_{ref}^{\beta oxi}}+v_x^L\frac{[GL_{HB}]}{L_{ref}^{\beta oxi}}\right)\left(\frac{[FA_H]}{K_{\beta oxi}^{FA}+[FA_H]}\right)\left(\frac{[atp]}{K_{\beta oxi}^{atp}+[atp]}\right)\left(1-\beta_{\beta oxi}^{aCoA}\frac{[aCoA]}{K_{\beta oxi}^{aCoA}+[aCoA]}\right)$
Lipogenesis	$Lgen$	$\mathcal{R}_{Lgen} = v_x^{Lgen}\left(1+v_x^{Ins}\frac{[Ins_{HB}]}{Ins_{ref}^{Lgen}}-v_x^L\frac{[GL_{HB}]}{L_{ref}^{Lgen}}\right)\left(\frac{[aCoA]}{K_{Lgen}^{aCoA}+[aCoA]}\right)\left(\frac{[atp]}{K_{Lgen}^{atp}+[atp]}\right)\left(1-\frac{[FA_H]}{K_{Lgen}^{FA}+[FA_H]}\right)$
Lipolysis	Lip	$\mathcal{R}_{Lip} = v^{Lip}\left(1-v_x^{Ins}\frac{[Ins_{HB}]}{Ins_{ref}^{Lip}}+v_x^L\frac{[GL_{HB}]}{L_{ref}^{Lip}}\right)\left(\frac{[TG_H]}{K_{Lip}^{TG}+[TG_H]}\right)$
Triglyceride Synthesis	$TSyn$	$\mathcal{R}_{TSyn} = v^{TSyn}\left(1+v_x^{Ins}\frac{[Ins_{HB}]}{Ins_{ref}^{TSyn}}-v_x^L\frac{[GL_{HB}]}{L_{ref}^{TSyn}}\right)\left(\frac{[FA_H]}{K_{TSyn}^{FA}+[FA_H]}\right)\left(\frac{[g3p]}{K_{TSyn}^{g3p}+[g3p]}\right)$
Glycerol Kinase	$GlyK$	$\mathcal{R}_{GlyK} = v^{GlyK}\left(\frac{[gly_H]}{K_{GlyK}^{gly}+[gly_H]}\right)\left(\frac{[atp]}{K_{GlyK}^{atp}+[atp]}\right)$
Adenosine Tri-phosphate Synthesis	$ATPS$	$\mathcal{R}_{ATPS} = v_x^{ATPS}\left(\frac{[aCoA]}{K_{ATPS}^{aCoA}+[aCoA]}\right)\left(\frac{[adp]}{K_{ATPS}^{adp}+[adp]}\right)\left(\frac{[P]}{K_{ATPS}^{P}+[P]}\right)\left(\frac{[Oxy_{HB}]}{K_{ATPS}^{Oxy}+[Oxy_{HB}]}\right)$
Uridine Diphosphate Kinase	$NDKU$	$\mathcal{R}_{NDKU} = v^{NDKU}\left(\frac{[atp][udp]}{(K_{NDKU}^{atp}+[atp])(K_{NDKU}^{udp}+[udp])}-\frac{[adp][utp]}{(K_{NDKU}^{adp}+[adp])(K_{NDKU}^{utp}+[utp])}\right)$
Guanosine Diphosphate Kinase	$NDKG$	$\mathcal{R}_{NDKG} = v^{NDKG}\left(\frac{[atp][gdp]}{(K_{NDKG}^{atp}+[atp])(K_{NDKG}^{gdp}+[gdp])}-\frac{[adp][gtp]}{(K_{NDKG}^{adp}+[adp])(K_{NDKG}^{gtp}+[gtp])}\right)$
Adenosine Kinase	AK	$\mathcal{R}_{AK} = v^{AK}\left(\frac{[atp][amp]}{(K_{AK}^{atp}+[atp])(K_{AK}^{amp}+[amp])}-\frac{[adp]^2}{(K_{AK}^{adp})^2+[adp]^2}\right)$
Additional Adenosine Tri-phosphate Use	$ATPu$	$\mathcal{R}_{ATPu} = v^{ATPu}\left(\frac{[atp]}{K_{ATPu}^{atp}+[atp]}\right)$
Control of Cellular Phosphate Levels	$PReg$	$\mathcal{R}_{PReg} = v^{PReg}([P]-P_{ref}^{PReg})$

Table 4: Metabolic processes represented in the hepatic compartment (H) and the given rate for the process (excluding transports between hepatic and hepatic blood compartments).

2.2 Systemic blood

It is in the representation and inclusion of metabolic processes in the systemic blood (referred to as the body compartment in [6, 7]) that the model presented here truly differs from the model in [6, 7] (excluding the addition of dispersion discussed in Section 2.3.2). These changes were made in order to improve biological detail as well as to simplify the equations here. Since the main focus of this model is on liver metabolism, we aim to leave these equations as simple as possible while keeping the concentrations at realistic levels. The main issue we came across was that the meal inputs were too significant of a driver of the system and resulted in metabolite concentrations falling too quickly in the absence of these inputs. To address this, we adjust the equations for the concentrations of metabolites and hormones in the systemic blood. A summary of the most significant changes is given below. Plots showing selected metabolite and hormone levels in the systemic blood before and after these changes are given in Figure 3. Equations for the concentrations in the systemic blood are given in Table 5 (note, $\mathcal{S}_{Ins}$ and $\mathcal{S}_{GL}$ are the rates of release of insulin and glucagon, respectively, by the pancreas. This takes the same form here as it does in [6], although constants may be changed).

Molecule	Equation
Glycerol	$\frac{d[gly_{SB}]}{dt} = Q_S([gly_{HB}(L,t)] - [gly_{SB}]) + \frac{1}{3}\mathcal{S}_{AdLip}$
Triglyceride	$\frac{d[TG_{SB}]}{dt} = Q_S([TG_{HB}(L,t)] - [TG_{SB}]) + s_{TG}\mathcal{S}_{Meal} - \frac{\ln 2}{\lambda}[TG_{SB}]$
Fatty acid	$\frac{d[FFA_{SB}]}{dt} = Q_S([FA_{HB}(L,t)] - [FA_{SB}]) + \mathcal{S}_{AdLip} - c_f[FA_{SB}]$
Glucose	$\frac{d[gC_{SB}]}{dt} = Q_S([gC_{HB}(L,t)] - [gC_{SB}]) + \mathcal{S}_{Meal} - \mathcal{S}_{gCup}$
Lactate	$\frac{d[Lac_{SB}]}{dt} = Q_S([Lac_{HB}(L,t)] - [Lac_{SB}])$
Insulin	$\frac{d[Ins_{SB}]}{dt} = Q_S([Ins_{HB}(L,t)] - [Ins_{SB}]) + s_{Ins}\mathcal{S}_{Ins} + b_{Ins}$
Glucagon	$\frac{d[GL_{SB}]}{dt} = Q_S([GL_{HB}(L,t)] - [GL_{SB}]) + s_{GL}\mathcal{S}_{GL}$
Oxygen	$\frac{d[Oxy_{SB}]}{dt} = Q_S([Oxy_{HB}(L,t)] - [Oxy_{SB}]) + c_{Oxy}$

Table 5: Equations for systemic blood concentrations (SB).

2.2.1 Glucose uptake in body

In the original model, glucose uptake in the rest of the body is represented by a function $\tilde{\mathcal{S}}_{gCup}$ dependent on plasma glucose level alone. This function takes the form of a simple Hill function given by

$$\tilde{\mathcal{S}}_{gCup} = \frac{v[gC_{SB}]}{K_M + [gC_{SB}]}. \tag{2}$$

While there is insulin independent glucose uptake in the body such as in the brain, the uptake of glucose in other tissues (such as muscle and adipose) does depend upon insulin [20, 76]. For this reason, we formulated a second term for the rate of insulin dependent glucose uptake in the body using Hill functions. Our resulting function for the rate of glucose uptake in the rest of the body is given by

$$\mathcal{S}_{gCup} = \frac{v_1[gC_{SB}]^{n_1}}{K_{M_1}^{n_1} + [gC_{SB}]^{n_1}} + v_2\left(\frac{[Ins_{SB}]^{n_I}}{K_{M_I}^{n_I} + [Ins_{SB}]^{n_I}}\right)\left(\frac{[gC_{SB}]^{n_2}}{K_{M_2}^{n_2} + [gC_{SB}]^{n_2}}\right). \tag{3}$$

The parameters for this function were estimated using a weighted least squares scheme with data from [26] and predictions were tested using data from [78] (see Figure 4). Finally, to get $\mathcal{S}_{gCup}$

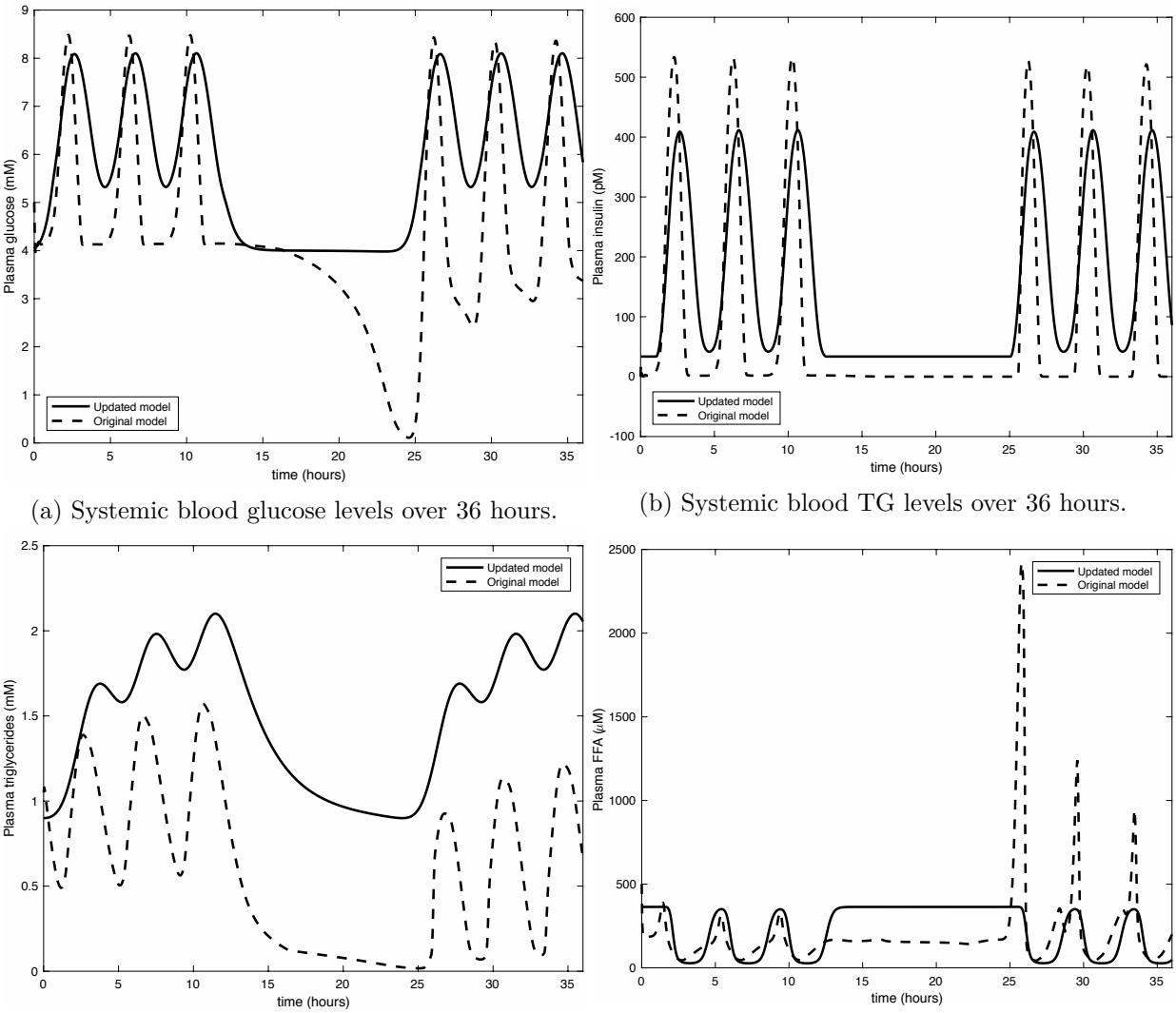

(a) Systemic blood glucose levels over 36 hours.

(b) Systemic blood TG levels over 36 hours.

(c) Systemic blood insulin levels over 36 hours.

(d) Systemic blood FA levels over 36 hours.

Figure 3: Concentrations in systemic blood before and after model changes.

in terms of the correct units for our model, we divide the rate by the volume of distribution of glucose, estimated to be 14L.

We note that the data used to estimate the parameters for $\mathcal{S}_{gCup}$ are extremely sparse and as such identifiability is nearly impossible to obtain from this data set alone. However, in this work we prioritize biological detail over identifiability concepts and as such assume our parameter estimates are sufficient with low confidence.

2.2.2 Lipolysis in adipose tissue

With no adipose compartment in the model, there is also no triglyceride storage in adipose tissue. In [6], plasma triglycerides are treated as adipose triglycerides for lipolysis in adipose tissue. To account for the fact that the size of the plasma triglyceride pool is much smaller than those stored

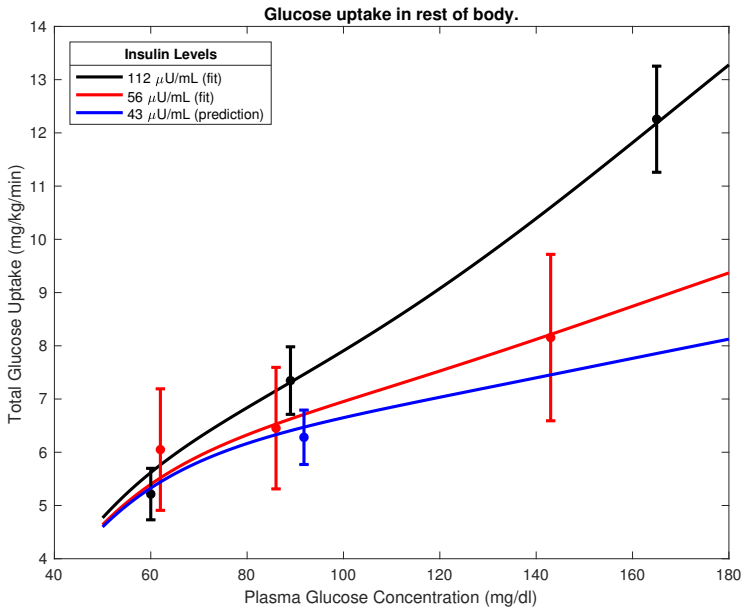

Figure 4: Data fit and model predictions for glucose uptake in rest of body.

in adipose tissue, rate constants that had a slow dependence upon plasma glucagon and insulin concentration were used. In our simulations, however, this adjustment to the rate constants did not prevent the plasma triglyceride pool from emptying during fasting periods (i.e., periods without meal inputs). To alleviate this, we take the rate of lipolysis in adipose tissue to be driven by insulin action alone. Figure 5 gives schematic representations of how lipolysis in adipose tissue is represented in the model from [6] (Figure 5a) and in the model given here (Figure 5b).

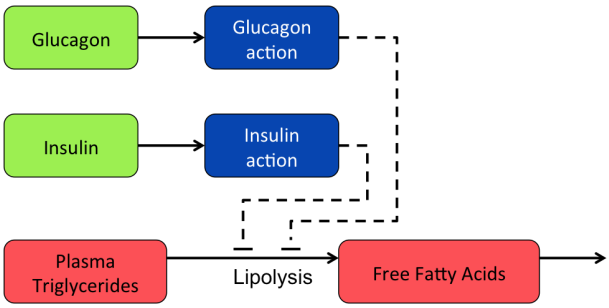

(a) Adipose lipolysis in [6].

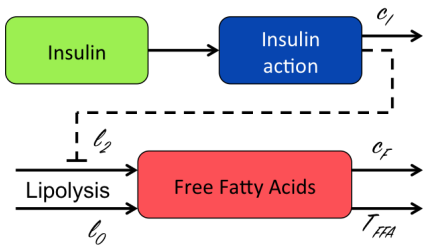

(b) Adipose lipolysis in model presented here.

Figure 5: Schematics of how adipose lipolysis is modeled.

Following the work of Periwal et al. [55, 65], we model the rate of lipolysis in adipose tissue with

the following system

$$\frac{d[FA_{SB}]}{dt} = L(I_A) - c_f[FA_{SB}] \tag{4a}$$

$$\frac{dI_A}{dt} = c_I([Ins_{SB}] - I_A - I_b) \tag{4b}$$

$$L(I_A) = l_0 + \frac{l_2}{1 + (I_A/I_{A2})^\alpha} \tag{4c}$$

where I_A is insulin action with initial condition $I_A(0) = 0$, $L = \mathcal{S}_{AdLip}$ is the rate of lipolysis, and c_f is general clearance of FFA to the body. This model was fit using data from [55] as well as mean parameter estimates and standard deviations provided therein as initial guesses and weights in a weighted least squares formulation. Figure 6 shows the fit to the FFA data where the model (4) was driven by insulin data.

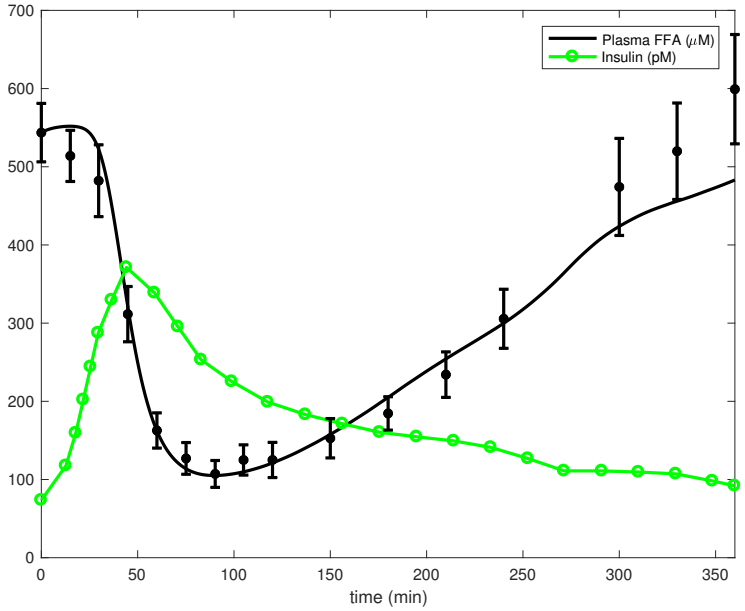

Figure 6: Data fit to (4).

Once the parameters for (4) were estimated, parameters for the transport as well as c_f were then adjusted so that approximately 30% of FFA being cleared to the body is transported to the liver. This amount is based on the percentage of palmitate cleared by the liver as indicated by data in [40].

2.2.3 Meal inputs

In [6], the meal inputs are given by a high-powered sine function (i.e., $v_{in}\sin^6(2\pi t/(2\text{ hours}))$ for some constant v_{in}). This representation for meal input causes sharp peaks with steep slopes in plasma glucose concentrations as well as other concentrations dependent on glucose (such as insulin). However, data shows [24, 25, 28] that the effect of meal ingestion upon concentrations of plasma metabolites should not give such a steep slope of decrease. These sharp peaks are largely due to the dynamics of the high-powered sine function which itself exhibits sharp peaks. Thus, to

reduce the slopes of the peaks in plasma glucose concentration (and other plasma metabolites), we represent the meal inputs using the solution to a basic differential equation (DE) that simulates the passage of food through the body (see Figure 7).

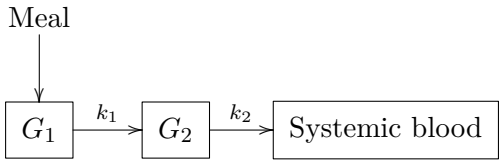

Figure 7: Schematic of meal input DE

The DE used to simulate meal ingestion is a two-compartment model where each compartment represents part of the gut and is given by

$$\begin{cases} \frac{dG_1}{dt} = -k_1 G_1 + \alpha G_{in} f_s, & G_1(0) = \alpha G_{in} \\ \frac{dG_2}{dt} = k_1 G_1 - k_2 G_2, & G_2(0) = 0. \end{cases} \tag{5}$$

The rate of change in plasma glucose from the ingestion of meals is then given by $\mathcal{S}_{meal} = k_2 G_2$. The source function, f_s is a Gaussian centered at two hours after the beginning of the meal. The meal cycle is: meals occur every 4 hours for 12 hours, then no meals for 12 hours (to simulate rest).

2.3 Hepatic Blood

In this paper, we will look at modeling the hepatic blood flow two different ways. One is modeling the blood flow as just a pure advective flow, which leads us to an advection-reaction (AR) equation for the concentrations of metabolites in the hepatic blood. The other is using Taylor's axial dispersion model which results in advection-dispersion-reaction (ADR) equations for the concentrations of metabolites in the hepatic blood. We perform simulations using both the AR and ADR equations and compare the results to determine whether or not the addition of dispersion in the blood flow, while more biologically accurate, has a significant effect upon the model solutions. The equations for both the AR system and the ADR system are given in Table 6. We note that we leave the equations for the hormones and oxygen the same for both models as they just give a basic gradient.

Mol.	AR Equation	ADR Equation
gly	$\frac{\partial [gly_{HB}]}{\partial t} = Q_H \frac{\partial [gly_{HB}]}{\partial x} - \gamma_H \mathcal{T}_{gly}$	$\frac{\partial [gly_{HB}]}{\partial t} = Q_H \frac{\partial [gly_{HB}]}{\partial x} - D_{gly} \frac{\partial^2 [gly_{HB}]}{\partial x^2} - \gamma_H \mathcal{T}_{gly}$
TG	$\frac{\partial [TG_{HB}]}{\partial t} = Q_H \frac{\partial [TG_{HB}]}{\partial x} - \gamma_H \mathcal{T}_{TG}$	$\frac{\partial [TG_{HB}]}{\partial t} = Q_H \frac{\partial [TG_{HB}]}{\partial x} - D_{TG} \frac{\partial^2 [TG_{HB}]}{\partial x^2} - \gamma_H \mathcal{T}_{TG}$
FA	$\frac{\partial [FA_{HB}]}{\partial t} = Q_H \frac{\partial [FA_{HB}]}{\partial x} - \gamma_H \mathcal{T}_{FA}$	$\frac{\partial [FA_{HB}]}{\partial t} = Q_H \frac{\partial [FA_{HB}]}{\partial x} - D_{FA} \frac{\partial^2 [FA_{HB}]}{\partial x^2} - \gamma_H \mathcal{T}_{FA}$
gC	$\frac{\partial [gC_{HB}]}{\partial t} = Q_H \frac{\partial [gC_{HB}]}{\partial x} - \gamma_H \mathcal{T}_{gC}$	$\frac{\partial [gC_{HB}]}{\partial t} = Q_H \frac{\partial [gC_{HB}]}{\partial x} - D_{gC} \frac{\partial^2 [gC_{HB}]}{\partial x^2} - \gamma_H \mathcal{T}_{gC}$
Lac	$\frac{\partial [Lac_{HB}]}{\partial t} = Q_H \frac{\partial [Lac_{HB}]}{\partial x} - \gamma_H \mathcal{T}_{Lac}$	$\frac{\partial [Lac_{HB}]}{\partial t} = Q_H \frac{\partial [Lac_{HB}]}{\partial x} - D_{Lac} \frac{\partial^2 [Lac_{HB}]}{\partial x^2} - \gamma_H \mathcal{T}_{Lac}$
Ins	$\frac{\partial [Ins_{HB}]}{\partial t} = Q_H \frac{\partial [Ins_{HB}]}{\partial x} - k_{Ins}[Ins_{HB}]$	$\frac{\partial [Ins_{HB}]}{\partial t} = Q_H \frac{\partial [Ins_{HB}]}{\partial x} - k_{Ins}[Ins_{HB}]$
GL	$\frac{\partial [GL_{HB}]}{\partial t} = Q_H \frac{\partial [GL_{HB}]}{\partial x} - k_{GL}[GL_{HB}]$	$\frac{\partial [GL_{HB}]}{\partial t} = Q_H \frac{\partial [GL_{HB}]}{\partial x} - k_{GL}[GL_{HB}]$
Oxy	$\frac{\partial [Oxy_{HB}]}{\partial t} = Q_H \frac{\partial [Oxy_{HB}]}{\partial x} - k_{Oxy}[Oxy_{HB}]$	$\frac{\partial [Oxy_{HB}]}{\partial t} = Q_H \frac{\partial [Oxy_{HB}]}{\partial x} - k_{Oxy}[Oxy_{HB}]$

Table 6: Equations for hepatic blood concentrations (HB).

2.3.1 Advection-Reaction (AR) Version

In [6, 7], the authors explain that they partition the hepatocytes around the sinusoid and blood flowing through the sinusoid into compartments depending upon where they lie on the sinusoid (see Figure 8). In this view, one might think of the model as multiple two compartment models that are connected by the blood flow through the hepatic blood compartments. This blood flow is modeled through a basic rate-in minus rate-out term. That is, supposing we've partitioned the hepatic blood into n compartments (note, in [6], these are referred to as "blood compartments"), if $[C_{HB}]_i$ is the concentration of metabolite C in hepatic blood compartment i, then the equation for $[C_{HB}]_i$ is given by

$$\frac{d[C_{HB}]_i}{dt} = v_{bf}([C_{HB}]_{i-1} - [C_{HB}]_i) - \gamma_H \mathcal{T}_i^C \tag{6}$$

for $i = 1, \ldots, n$. Here, γ_H is the ratio of hepatic to hepatic blood volume and $\mathcal{T}_i^C$ is the rate of transport of metabolite C between hepatic blood compartment i and hepatic compartment i. The rate of blood flow v_{bf} is given by

$$v_{bf} = Q_H n \tag{7}$$

per second, where $Q_H = 0.15$. This value for Q_H was chosen in order to make a circuit of blood flow last approximately 5 minutes [6]. Note then that we have

$$\frac{d[C_{HB}]_i}{dt} = \frac{Q_H}{1/n}([C_{HB}]_{i-1} - [C_{HB}]_i) - \gamma_H \mathcal{T}_i^C \tag{8}$$

and observe that

$$\frac{\partial[C_{HB}]_i}{\partial x} \approx \frac{Q_H}{1/n}([C_{HB}]_{i-1} - [C_{HB}]_i) \tag{9}$$

for $i = 1, \ldots, n$, is the first order upwind advection discretization on an uniform mesh. Thus, while the model in [6, 7] can be considered a compartments-in-series model comprised solely of ODE's, one can also view it as an advection-reaction equation strongly coupled to mass-balance equations describing the concentrations of metabolites in the liver cells (see Figure 2). That is, we allow $[C_{HB}]$ and $[C_H]$ to be spatially dependent and write

$$\frac{\partial[C_{HB}]}{\partial t} = Q_H \frac{\partial[C_{HB}]}{\partial x} - \gamma_H \mathcal{T}^C([C_{HB}], [C_H]). \tag{10}$$

We note that Q_H is in units $\frac{1}{\text{second}}$. That is, this advection equation is dimensionless in the axial direction. This implies that we can assume our sinusoid length is $L = 1$.

In [6, 7], when viewing the model as a compartments-in-series model, the authors treat the blood flow in the systemic blood (referred to in [6, 7] as the body compartment) similarly. If $[C_{HB}]_n$ is the concentration of metabolite C is the final compartment of the hepatic blood, and $[C_{SB}]$ is the concentration in the systemic blood, then

$$\frac{d[C_{SB}]}{dt} = \frac{Q_H}{\gamma_B}([C_{HB}]_n - [C_{SB}]) + \mathcal{S} \tag{11}$$

where γ_B is the ratio between the volume of systemic blood to the volume of hepatic blood, and $\mathcal{S}$ represents the metabolic processes included in the model from the rest of the body. When considering the concentrations of metabolites in the hepatic blood to be spatially dependent (rather

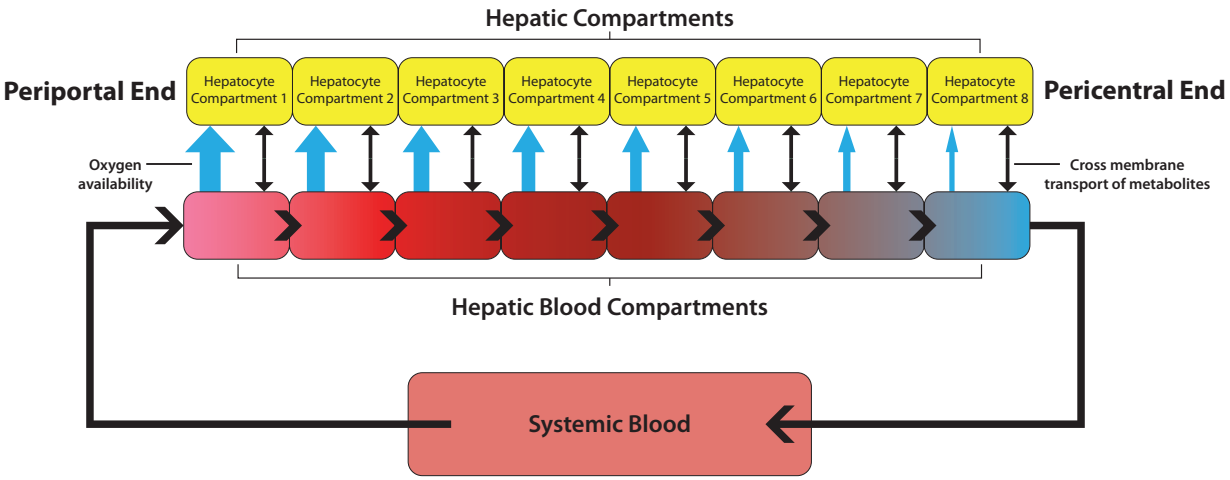

Figure 8: Schematic of compartments-in-series model.

than compartment dependent), the concentration of metabolites in the systemic blood actually become Dirichlet boundary conditions for the hepatic blood equations. Thus the dynamics of the concentration of metabolite C in the hepatic blood is given by

$$\frac{\partial [C_{HB}]}{\partial t} = Q_H \frac{\partial [C_{HB}]}{\partial x} - \gamma_H \mathcal{T}^C([C_{HB}], [C_H]), \qquad 0 < x < 1,\ t > 0, \tag{12}$$

$$[C_{HB}](0,t) = [C_{SB}](t), \qquad t > 0, \tag{13}$$

$$[C_{HB}](x,0) = f_{HB}, \qquad 0 < x < 1, \tag{14}$$

where f_{HB} represents the initial distribution of the concentration of metabolite C in the hepatic blood. Here, we keep the feedback loop by using the ODE

$$\frac{d[C_{SB}]}{dt} = \frac{Q_B}{\gamma_B}\left([C_{HB}](1,t) - [C_{SB}](t)\right) + \mathcal{S}, \tag{15}$$

with initial condition $[C_{SB}](0) = f_{SB}$ to obtain the value of $[C_{SB}]$.

2.3.2 Advection-Dispersion-Reaction (ADR) Version

While an AR equation such as the one given in Section 2.3.1 is a good model for simple flows, the actual dynamics of blood flow through a capillary are much more complex than just a pure advective flow. Here, we include the effect of the dispersion that occurs due to the flow by modeling the blood flow using Taylor's axial dispersion model [33]. This model has been used previously for blood flow through the liver sinusoid in other works such as [19, 22]. Here, we add a dispersion term to the AR model of Section 2.3.1 in order to get an advection-dispersion-reaction (ADR) equation in order to compare the two and thus *determine whether or not a dispersion term makes a significant difference for the model presented here (one of the goals of this presentation).*

The addition of a dispersion term, and thus the addition of a second spatial derivative, requires boundary conditions at both the periportal and pericentral ends of the sinusoid in order to remain well-posed (in contrast, the AR equation only requires boundary conditions at one end). To

accommodate this, we assign homogeneous Neumann conditions at the pericentral end to indicate that the concentration of the metabolite leaving the sinusoid is the same as the concentration entering the systemic blood. The concentration of metabolite C in the hepatic blood is now given by

$$\frac{\partial[C_{HB}]}{\partial t} = Q_H \frac{\partial[C_{HB}]}{\partial x} - D_C \frac{\partial^2[C_{HB}]}{\partial x^2} - \gamma_H \mathcal{T}^C([C_{HB}], [C_H]), \qquad 0 < x < 1,\, t > 0, \quad (16)$$

$$[C_{HB}](0,t) = [C_{SB}](t), \qquad t > 0, \quad (17)$$

$$\frac{\partial[C_{HB}]}{\partial x}(1,t) = 0, \qquad t > 0, \quad (18)$$

$$[C_{HB}](x,0) = f_{HB}, \qquad 0 < x < 1, \quad (19)$$

where D_C is the dispersion coefficient of metabolite C in blood and everything else is defined as in Section 2.3.1 (including the equation for $[C_{SB}]$).

Determining the appropriate values for D_C is nontrivial due to the fact that Q_H is dimensionless in the axial direction. This implies that we need D_C to be dimensionless in the axial direction as well. The difficulty here is the requirement to keep things scaled appropriately with respect to the biology without knowing the scaling factor used to render the AR equations dimensionless. In order to determine an appropriate scaling factor, we must look more closely at the role of v_{bf} in the model from [6, 7].

If n is the number of compartments the hepatic blood has been separated into (in [6, 7], these are referred to as the blood compartments), then

$$v_{bf} = \frac{\text{rate of blood flow in the liver}}{\text{volume of blood compartment}}. \quad (20)$$

In general, the rate of blood flow in the liver is given by the volume of blood in the liver divided by the time it takes the blood to go through the liver. Since the volume of a blood compartment should be the volume of blood in the liver divided by n (the number of compartments), we get that

$$v_{bf} = \frac{n}{\text{time it takes blood to go through the liver}}. \quad (21)$$

Thus, from (7), we have that, under this scaling, the time it takes blood to go through the liver is $\frac{1}{Q_H}$ seconds.

In order to have an unscaled advection equation, we would need to know the velocity of the blood in the liver. Let v be this velocity. Then

$$v = \frac{\text{distance traveled through liver}}{\text{time it takes blood to go through the liver}} = \frac{L}{1/Q_H} \quad (22)$$

or

$$v = Q_H L. \quad (23)$$

Now, while our model is of the liver microstructure (that is of a liver sinusoid and the surrounding cells), the concentrations of metabolites our model gives is actually representative of the accumulation from all sinusoids in the liver. On the other hand, in [22], the authors model the production from a single sinusoid using Taylor's axial dispersion and using physical measurements for the

length of the sinusoid, velocity of blood, etc. Assuming then that our model gives us the concentration from a single sinusoid times the number of sinusoids in the liver, one can obtain that we should have $v = v_{sin}$ and $D_C^s = D_C^{sin}$ where v_{sin} and D_C^{sin} are the velocity of blood and dispersion coefficient in a single sinusoid respectively and D_C^s is the unscaled dispersion coefficient for our model. In [22] $L_{sin} = 1$mm is used as the length of the sinusoid and $\tau = 5.4$ seconds is assumed to be the time it takes blood to get through a sinusoid. Thus, we can calculate

$$L = \frac{v}{Q_H} = \frac{L_{sin}}{Q_H \tau} = 1.23\text{mm}. \tag{24}$$

Now that we have our scaling factor L, we can follow the process and values in [22] to compute D_C^{sin} and then divide by L^2 in order to obtain the scaled dispersion coefficient D_C that we will use in our simulations. That is, we use Renkin's equation [35]

$$D_C^i = 1.013 \times 10^{-4} \times (MW)^{-0.46} \frac{\text{cm}^2}{s} \tag{25}$$

to compute the diffusion coefficient D_C^i using the molecular weight MW of C. We then use the Aris-Taylor's relation [33]

$$D_C^{sin} = D_C^i + \frac{\left(\frac{v_{sin} d_s}{2}\right)^2}{48 D_C^i} \tag{26}$$

to calculate D_C^s (where d_s is the diameter of the sinusoid (given in [22])). Finally, we scale the dispersion coefficient to obtain

$$D_C = \frac{D_C^s}{L^2}. \tag{27}$$

3 Results

Discretization in space is carried out using a first-order upwind difference for the advection term and a second-order central difference for the dispersion term. The resulting ODE's are then solved using ode15s from the Matlab ODE suite.

First, we look at how varying the mesh size $h = 1/n$ affects the numerical solutions of the AR version of the model (equivalently, seeing how varying the number of compartments n affects the compartments-in-series ODE model). Figure 9 shows some of the metabolite levels at the time when the difference between the metabolite levels from the most coarse grid used ($n = 5$) and the most fine grid used ($n = 500$) is largest. While the change in the metabolite levels from varying n can be rather small in some cases (e.g. change in hepatic blood glucose levels only reaches $0.37 - 0.43\%$ of the span of hepatic blood glucose levels), in other cases it is much larger as can be seen from Table 7 which shows the largest change seen in the metabolites due to varying n from 5 to 500 using 72 hour simulations. We note that since the span of the metabolite levels varies depending upon where the level is taken on the sinusoid, these changes were calculated separately for each spatial grid point on the coarse grid (in this case, $n = 5$) and the span given in Table 7 contains the largest changes in the metabolite level at each coarse grid point.

The differences seen due to the mesh size (or number of compartments) can be explained by the addition of numerical dispersion in the hepatic blood equations through the first-order upwind

Variable	Largest change	Variable	Largest change	Variable	Largest change
gC_{HB}	$0.37 - 0.43\%$	gC_H	$1.01 - 2.73\%$	gdp	$9.91 - 31.7\%$
TG_{HB}	$0.91 - 0.92\%$	TG_H	$2.91 - 61.5\%$	gtp	$9.91 - 31.7\%$
FA_{HB}	$6.94 - 7.00\%$	FA_H	$8.07 - 28.5\%$	udp	$3.87 - 10.9\%$
gly_{HB}	$6.87 - 17.4\%$	gly_H	$3.51 - 28.2\%$	utp	$3.87 - 10.9\%$
Lac_{HB}	$7.48 - 8.00\%$	Lac_H	$7.12 - 17.1\%$	adp	$15.4 - 54.7\%$
Oxy_{HB}	$16.0 - 80.6\%$	G	$4.57 - 42.2\%$	atp	$11.1 - 26.2\%$
GL_{HB}	$6.43 - 9.94\%$	$g6p$	$3.47 - 36.9\%$	amp	$10.5 - 26.1\%$
Ins_{HB}	$5.87 - 14.9\%$	$g3p$	$9.94 - 35.8\%$	P	$8.57 - 61.4\%$
				$aCoA$	$10.9 - 38.0\%$

Table 7: Change of metabolite levels in over x from refining the mesh from $n = 5$ to $n = 500$ (relative to overall range of metabolite level).

advection discretization. It can be shown that while the first-order upwind scheme is first-order accurate to the advection equation

$$u_t + au_x = 0, \tag{28}$$

it is actually second-order accurate to the modified advection-dispersion equation

$$\tilde{u}_t + a\tilde{u}_x = \frac{1}{2}ah\tilde{u}_{xx}, \tag{29}$$

where a is the advection coefficient and h the mesh size [43]. Thus, the amount of numerical dispersion being introduced in the numerical solution is directly related to the mesh size (or number of compartments). We see further that the change in the hepatic blood metabolite levels also has a strong affect on the hepatic metabolite levels seen through the large changes seen in these levels (Table 7, two middle and two right columns). This is likely due to the strength of the coupling between these sets of equations. We also note that, regardless of the addition of numerical dispersion, it appears that if the mesh size h is not sufficiently small (or number of compartments n sufficiently large), then interesting spatial dynamics of the levels in the hepatocytes may be lost as can be seen by Figures 9e and 9f.

Secondly, we want to investigate how the intentional inclusion of dispersion affects the system. That is, we wish to compare the AR simulation results with the ADR simulation results. In an attempt to limit the effect of numerical dispersion from the advection term while keeping computation time fairly short, we use $n = 50$ compartments (or a mesh size of $h = 1/50$). From Figure 9 it appears that most of the metabolite levels start to converge around $n = 50$. Further, Table 8 shows that the changes in all metabolite levels between $n = 50$ and $n = 500$ is less that 10% the span of the metabolite.

Figure 10 depicts the metabolite levels across the sinusoid at the time for which the solutions to the AR and ADR versions of the model have the largest difference for each particular metabolite (as measured by the discrete 2 norm). As can be seen from Figure 10, there does not appear to be a significant difference between the solutions from the AR and ADR versions of the model. Further the differences are small in comparison to the span of the metabolite levels over time as can be seen from Table 9. This indicates that the addition of dispersion may not have a

Variable	Largest change	Variable	Largest change	Variable	Largest change
gC_{HB}	$0.0342 - 0.0386\%$	gC_H	$0.052 - 0.38\%$	gdp	$0.82 - 3.10\%$
TG_{HB}	$0.0832 - 0.0835\%$	TG_H	$0.21 - 5.88\%$	gtp	$0.82 - 3.10\%$
FA_{HB}	$0.65 - 0.66\%$	FA_H	$0.58 - 2.76\%$	udp	$0.18 - 1.16\%$
gly_{HB}	$0.63 - 1.69\%$	gly_H	$0.30 - 3.29\%$	utp	$0.18 - 1.16\%$
Lac_{HB}	$0.59 - 0.68\%$	Lac_H	$0.62 - 1.74\%$	adp	$1.42 - 4.39\%$
Oxy_{HB}	$1.48 - 7.76\%$	G	$0.065 - 4.21\%$	atp	$0.69 - 2.42\%$
GL_{HB}	$0.60 - 0.93\%$	$g6p$	$0.32 - 7.11\%$	amp	$0.70 - 2.41\%$
Ins_{HB}	$0.53 - 1.37\%$	$g3p$	$0.83 - 3.63\%$	P	$0.70 - 5.81\%$
				$aCoA$	$0.57 - 3.80\%$

Table 8: Change of metabolite levels over x from refining the mesh from $n = 50$ to $n = 500$ (relative to overall range of metabolite level).

significant effect on the metabolite levels. However, we note that the presence of numerical dispersion could be muffling the effect of the actual dispersion. In fact, in these simulations the numerical dispersion is on the order of 10^{-3} while the actual dispersion is only on the order of 10^{-4}. Thus, though the actual dispersion does not have much of an effect in these numerical simulations, other discretizations could unveil the dispersion to have a larger effect than seen here.

Variable	Largest change	Variable	Largest change	Variable	Largest change
gC_{HB}	$0.434 - 0.527\%$	gC_H	$0.438 - 0.520\%$	gdp	$0.279 - 1.557\%$
TG_{HB}	$0.135 - 0.136\%$	TG_H	$0.251 - 0.656\%$	gtp	$0.279 - 1.557\%$
FA_{HB}	$0.7698 - 0.723\%$	FA_H	$0.360 - 0.976\%$	udp	$1.27 - 1.49\%$
gly_{HB}	$0.705 - 1.37\%$	gly_H	$0.763 - 1.72\%$	utp	$1.27 - 1.49\%$
Lac_{HB}	$1.35 - 2.10\%$	Lac_H	$1.10 - 1.90\%$	adp	$0.325 - 1.52\%$
Oxy_{HB}	0.505e-4 $-$ 3.82e-4%	G	$0.719 - 0.940\%$	atp	$0.380 - 1.27\%$
GL_{HB}	$0.258 - 0.493\%$	$g6p$	$0.375 - 0.670\%$	amp	$0.358 - 1.26\%$
Ins_{HB}	$0.761 - 0.765\%$	$g3p$	$0.535 - 1.63\%$	P	$0.153 - 0.579\%$
				$aCoA$	$0.338 - 0.979\%$

Table 9: Change of metabolite levels over x between AR and ADR simulation (relative to overall range of AR simulation metabolite level).

Lastly, under this discretization, it appears that including the dispersion term actually increases computation time exponentially. Simulations were run using various mesh sizes (from $h = 1/5$ to $h = 1/50$) and computation times were recorded. Figure 11 illustrates the ADR computation times as a function of the AR computation times. The Matlab function lsqcurvefit was used to fit an exponential to this data and, at least empirically, appears to capture the trend quite well. The fit exponential is given by

$$t_{ADR} = 0.1720e^{0.3119t_{AR}} \tag{30}$$

where t_{ADR} and t_{AR} are computation times for the ADR and AR systems respectively.

4 Conclusions

In this paper, we investigate the effect the number of compartments used in a model of the liver microstructure similar to the one presented in [6, 7] has on the simulated concentrations as well as how including dispersion affects the system. The model of the liver microstructure from [6, 7] was adjusted in order to keep metabolic levels realistic when the system is not being driven by meal inputs. This adjustment included, most influentially, the addition of insulin dependent glucose uptake in the body excluding the liver, rate of lipolysis in adipose tissue depending solely upon insulin action, and representation of meal inputs as the solution to a two-compartment model of ingestion in the gut. The model in [6, 7] is presented as a compartments-in-series model, however we present it here as a system of advection-reaction equations that give the dynamics of concentrations in the hepatic blood, coupled to mass-balance equations that provide dynamics for the concentrations in the hepatic tissue. The in-flow boundary condition for the hepatic blood equations is given by the solution to an ODE that yields a basic representation of metabolism in the rest of the body which depends upon the out-flow concentrations, hence creating a feedback loop. The reason for this difference in representation is the fact that the equations for concentrations in the hepatic blood in the compartments-in-series model given in [6, 7] are equivalent to advection-reaction equations that have been spatially discretized using a upwind forward difference and a mesh size of $h = 1/8$ (corresponding to $n = 8$ compartments).

Numerical simulations were carried out using the upwind forward difference discretization for the advection term in order to investigate how changing the number of compartments n affects the compartments-in-series model. We find that the value of n does have a large affect on the simulated concentrations, as can be seen from Table 7. One of the advantages of viewing this system as a PDE as opposed to a compartments-in-series ODE is the ability to analyze the numerical simulations in terms of spatial discretization. Indeed, by analyzing the modified equation (29) we see that numerical dispersion has been introduced into the solution, the amount of which has an inverse relationship with the number of compartments n. Interestingly, we find that the value of n has, in many cases, an even larger affect on the hepatic concentrations than on the hepatic blood concentrations. This seems counter intuitive as there is no spatial discretization in the equations for hepatic concentrations, thus no numerical dispersion is directly introduced to these concentrations. Thus, the numerical dispersion can only affect these concentrations indirectly through the coupling of the hepatic blood to the hepatic equations. This, then, is a testament to the strength of the coupling in the system, both between hepatic and hepatic blood variables as well as between the hepatic variables themselves since not all hepatic equations are directly coupled to a hepatic blood equation.

We also address how intentionally included dispersion affects the system. This is of interest because it is biologically more accurate and has been included in other models of the liver microstructure. Most notably, Berndt et al. [11] include a dispersive affect in the blood flow of their compartments-in-series model. When looked at closely, one sees that this dispersion is in fact modeled through a second-order central difference discretization for a standard dispersion term (that is, a discretization for $\frac{\partial^2}{\partial x^2}$). We use the same discretization in our simulations here and find that the inclusion of dispersion does not appear to have a significant affect on our system (see Table 9). Further, the addition of dispersion appears to increase computation time exponentially. Thus, we conclude that for models discretized in this way, it is more efficient to use just the AR version over the ADR version. However, we note that the numerical dispersion is dominating the

actual dispersion, and is thus likely muting the effect of the actual dispersion. If we consider the system as a PDE system, then we can utilize more accurate spatial discretizations in order to better analyze the effect of dispersion. Advection-dispersion equations are known to be difficult to solve numerically and every discretization has its pros and cons [43]. However, because of this there is a wide breadth of research on how to solve these systems numerically, and as such there is an abundance of existing algorithms one could utilize. Unfortunately, the size of the system considered in this paper along with the stiffness and strong coupling of the system make other discretizations difficult to implement and computationally costly. Because of this, we recommend testing other discretizations on a smaller system that has the same form as the one considered here. This preliminary study on a smaller system will lend valuable insights into what numerical scheme will be most effective for systems of this type.

In the past, arguments have been made for compartments-in-series models over PDE models for hepatic elimination often citing the mathematical simplicity of ODEs compared to PDEs [4, 38]. However, many of these compartments-in-series models are equivalent to a spatially discretized PDE, especially in how they've been used thus far to model liver metabolism. Thus, considering these models strictly as ODEs is potentially limiting the information and insights these systems may be able to give us. In particular, if our goal is to understand why and how certain spatially dependent processes occur, such as metabolic zonation and the phenomena of zonated steatosis in liver disease, then it makes sense to consider systems of PDEs which give us more options when it comes to discretizing spatially in numerical schemes. Further, PDEs lends themselves more appropriately in this problem to theoretical analyses that can unveil properties of the system such as the functional framework and stability. Compartments-in-series models are very useful computational tools and considering these systems from the perspective of a PDE does not diminish that. Rather, it provides more options and tools with which to analyze the system, both numerically and theoretically.

Acknowledgments

This research was supported in part by the Air Force Office of Scientific Research (HTB, MN) under grant number AFOSR FA9550-18-1-0457 and in part by a CRSC/Lord Corporation Fellowship (MN).

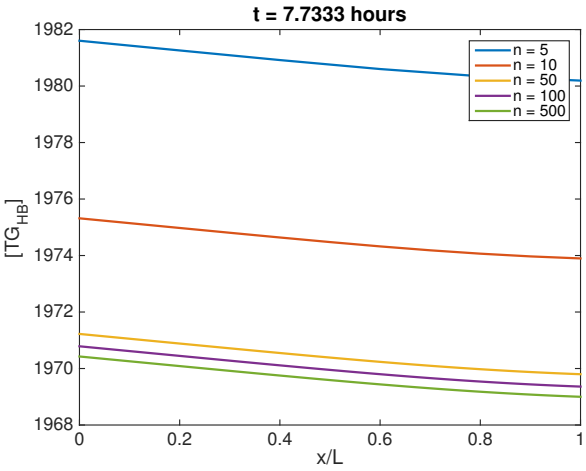

(a) Hepatic blood TG levels at 7.73 hours.

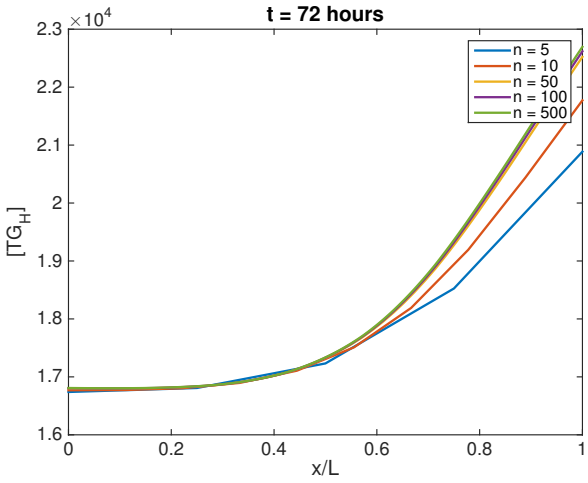

(b) Hepatic TG levels at 72 hours.

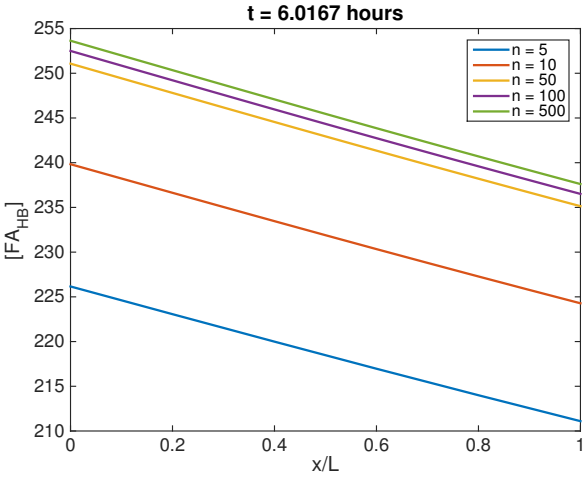

(c) Hepatic blood FA levels at 6.02 hours.

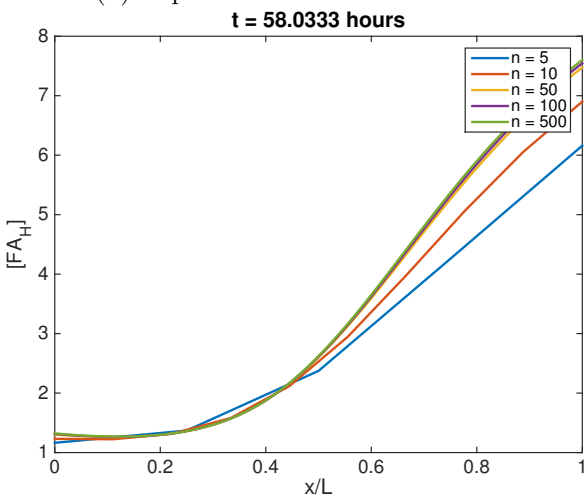

(d) Hepatic FA levels at 58.03 hours.

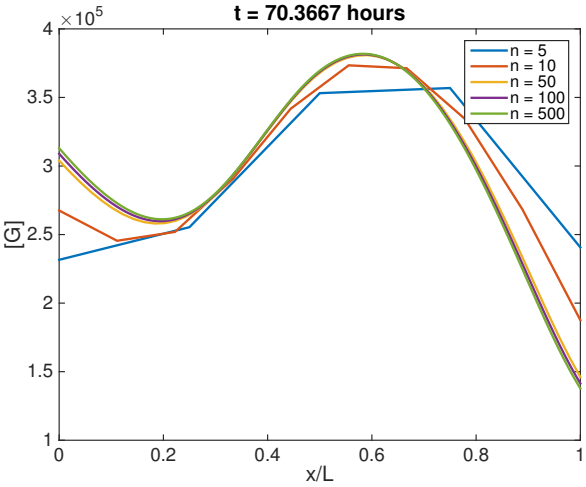

(e) Glycogen levels at 70.37 hours.

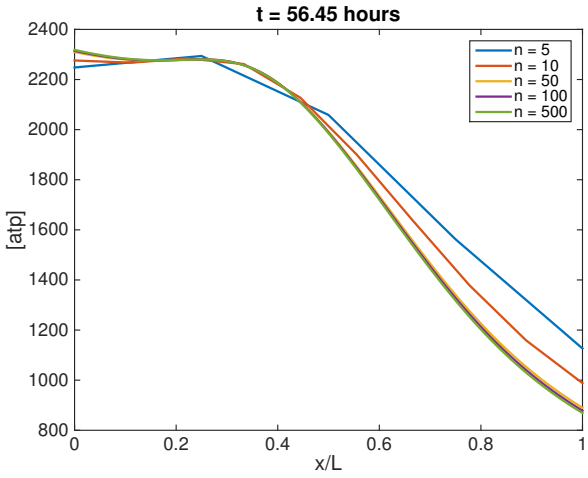

(f) Atp levels at 56.45 hours.

Figure 9: Metabolite levels for various mesh sizes across the sinusoid at time of largest difference between $h = 1/5$ and $h = 1/500$ (72 hour simulations).

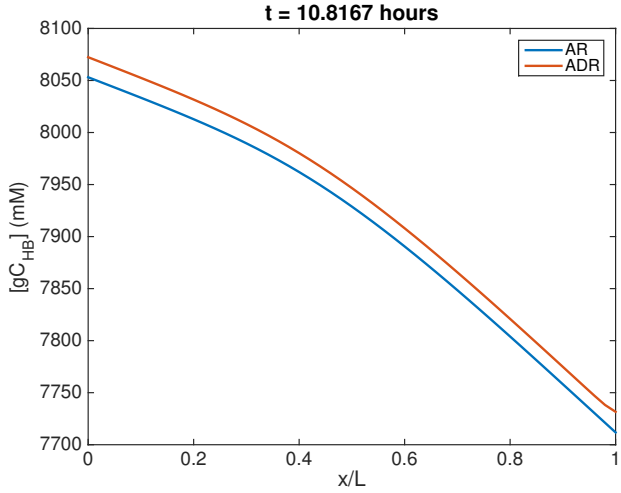

(a) Hepatic blood glucose levels at 10.82 hours.

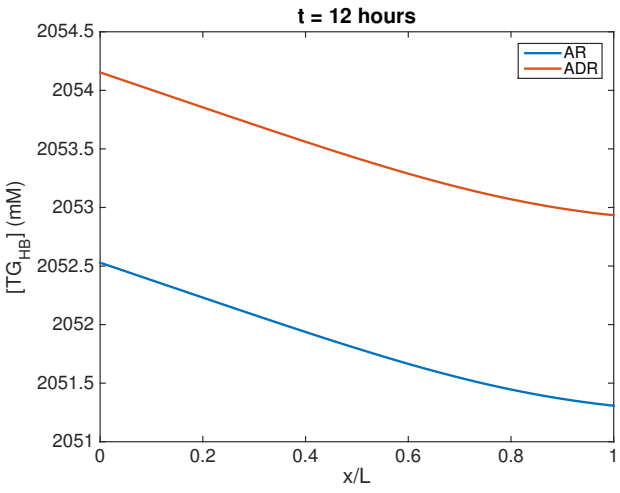

(b) Hepatic blood TG levels at 12 hours.

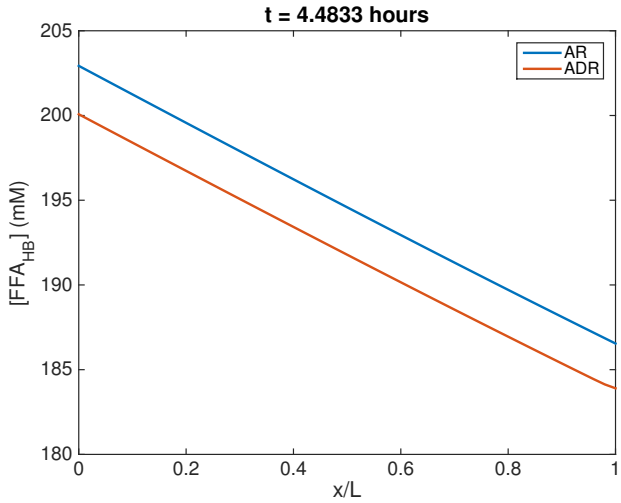

(c) Hepatic blood FA levels at 4.48 hours.

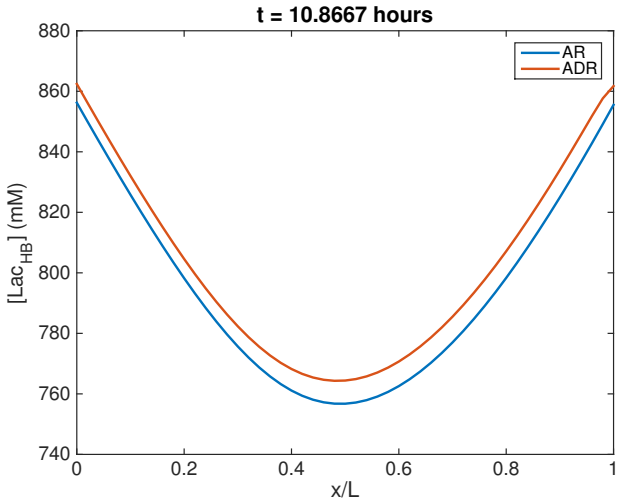

(d) Hepatic blood lactate levels at 10.87 hours.

Figure 10: Metabolite levels for AR and ADR versions of the model across the sinusoid at time of largest difference (24 hour simulations).

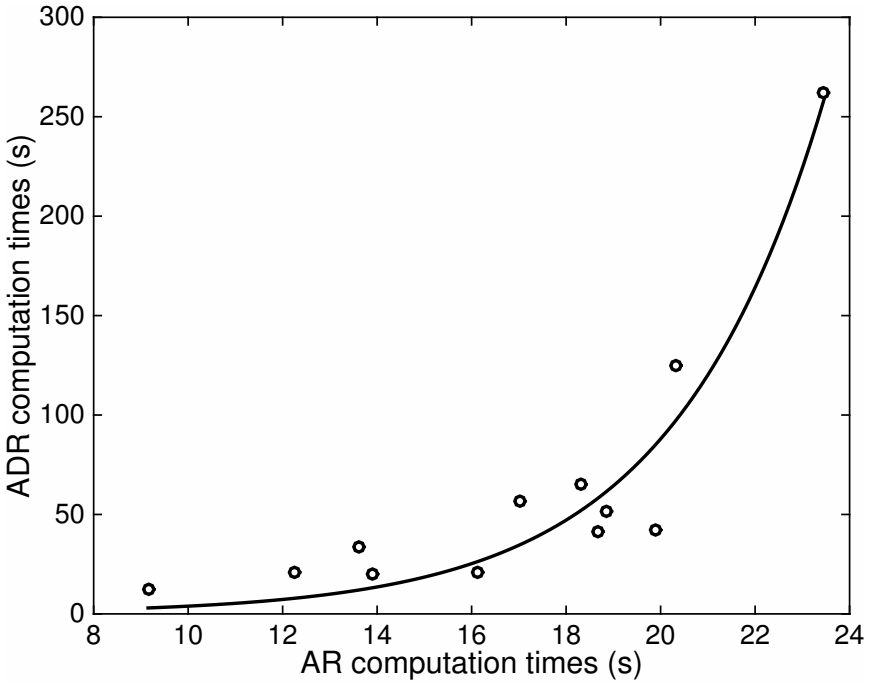

Figure 11: Computational times of ADR against AR with exponential fit.

References

[1] Abdelmalek, M.F., Diehl, A.M. (2007). Nonalcoholic fatty liver disease as a complication of insulin resistance. *Med. Clin. North Am.* 91(6): 1125-1149. doi: 10.1016/j.mcna.2007.06.001

[2] Adams, L.A., Angulo, P., Lindor, K.D. (2005). Nonalcoholic fatty liver disease. *CMAJ* 172: 899-905. doi.org/10.1503/cmaj.045232

[3] Anderson, C.M., Stahl, A. (2013). SLC27 fatty acid transport proteins. *Mol. Aspects Med.* 34(2-3): 516-528. doi.org/10.1016/j.mam.2012.07.010

[4] Anissimov, Y.G., Roberts, M.S. (2002). A compartmental model of hepatic disposition kinetics: 1. Model development and application to linear kinetics. *J. Pharmacokinet. Pharmacodyn.* 29(2): 131-156.

[5] Arab, J.P., Arrese, M., Trauner, M. (2018). Recent insights into the pathogenesis of nonalcoholic fatty liver disease. *Annu. Rev. Pathol. Mech. Dis.* 13: 321-350. doi.org/10.1146/annurev-pathol-020117-043617

[6] Ashworth, W.B., Davis, N.A., Bogle, I.D.L. (2016). A computational model of hepatic energy metabolism: understanding zonated damage and steatosis in NAFLD. *PLoS Comput. Biol.* 12(9): e1005105. doi.org/10.1371/journal.pcbi.1005105

[7] Ashworth, W.B., Perez-Galvan, C., Davies, N.A., Bogle, I.D.L. (2016). Liver function as an engineering system. *AIChE J.* 62(9): 3285-3297. doi.org/10.1002/aic.15292

[8] Banini, B.A., Sanyal, A.J. (2016). Nonalcoholic fatty liver disease: epidemiology, pathogenesis, natural history, diagnosis, and current treatment options. *Clin. Med. Insights Ther.* 8: 75-84. doi.org/10.4137/CMT.S18885

[9] Bass, L., Keiding, S., Winkler, K., Tygstrup, N. (1976). Enzymatic elimination of substrates flowing through the intact liver. *J. Theor. Biol.* 61: 393-409.

[10] Bass, L., Robinson, P., Bracken, A.J. (1978). Hepatic elimination of flowing substrates: the distributed model. *J. Theor. Biol.* 72: 161-184.

[11] Berndt, N., Horger, M.S., Bulik, S., Holzhütter, H.-G. (2018). A multiscale modelling approach to assess the impact of metabolic zonation and microperfusion on the hepatic carbohydrate metabolism. *PLoS Comput. Biol.* 14(2): e1006005. doi.org/10.1371/journal.pcbi.1006005

[12] Bhatia, S.N., Toner, M., Foy, B.D., Rotem, A., O'Neil, K.M., Tompkins, R.G., Yarmush, M.L. (1996). Zonal liver cell heterogeneity: effects of oxygen on metabolic functions of hepatocytes. *Cell. Eng.* 1: 125-135.

[13] Black, P.N., Ahowesso, C., Montefusco, D., Saini, N., DiRusso, C.C. (2016). Fatty acid transport proteins: targeting FATP2 as a gatekeeper involved in the transport of exogenous fatty acids. *Medchemcomm* 7(4): 612-622. doi.org/10.1039/C6MD00043F

[14] Black, P.N., Sandoval, A., Arias-Barrau, E., DiRusso, C.C. (2009). Targeting the fatty acid transport proteins (FATP) to understand the mechanisms linking fatty acid transport to metabolism. *Immunol. Endocr. Metab. Agents Med. Chem.* 9(1): 11-17.

[15] Brunt, E.M. (2010). Pathology of nonalcoholic fatty liver disease. *Nat. Rev. Gastroenterol. Hepatol.* 7: 195-203. doi.org/10.1038/nrgastro.2010.21

[16] Brunt, E.M. (2007). Pathology of fatty liver disease. *Mod. Pathol.* 20(1 Suppl): S40-S48.

[17] Brunt, E.M., Janney, C.G., Di Bisceglie, A.M., Neuschwander-Tetri, B.A., Bacon, B.R. (1999). Nonalcoholic steatohepatitis: a proposal for grading and staging the histological lesions. *Am. J. Gastroenterol.* 94: 2467-2474. doi.org/10.1111/j.1572-0241.1999.01377.x

[18] Buqué, X., Cano, A., Miquilena-Colina, M.E., García-Monzón, C., Ochoa, B., Aspichueta, P. (2012). High insulin levels are required for FAT/CD36 plasma membrane translocation and enhanced fatty acid uptake in obese Zucker rat hepatocytes. *Am. J. Physiol. Endocrinol. Metab.* 303: E504-E514. doi.org/10.1152/ajpendo.00653.2011

[19] Calvetti, D., Kuceyeski, A., Somersalo, E. (2008). Sampling-based analysis of a spatially distributed model for liver metabolism at steady state. *Multiscale Model. Simul.* 7(1): 407-431.

[20] Cartee, G.D. (2015). Mechanisms for greater insulin-stimulated glucose uptake in normal and insulin-resistant skeletal muscle after acute exercise. *Am. J. Physiol. Endocrinol. Metab.* 309(12): E949-E959. doi.org/10.1152/ajpendo.00416.2015

[21] Chalasani, N., Wilson, L., Kleiner, D.E., Cummings, O.W., Brunt, E.M., Ünalp A (2008). Relationship of steatosis grade and zonal location to histological features of steatohepatitis in adult patients with non-alcoholic fatty liver disease. *J. Hepatol.* 48: 829-834. doi.org/10.1016/j.jhep.2008.01.016

[22] Chalhoub, E., Xie, L., Balasubramanian, V., Kim, J., Belovich, J. (2007). A distributed model of carbohydrate transport and metabolism in the liver during rest and high-intensity exercise. *Ann. Biomed. Eng.* 35(3): 474-491.

[23] Colletti, M., Cicchini, C., Conigliaro, A., Santangelo, L., Alonzi, T., Pasquini, E., Tripodi, M., Amicone, L. (2009). Convergence of Wnt signaling on the HNF4α-driven transcription in controlling liver zonation. *Gastroenterology* 137(2): 660-672. doi.org/10.1053/j.gastro.2009.05.038

[24] Coppack, S.W., Fisher, R.M., Gibbons, G.F., Humphreys, S.M., McDonough, M.J., Potts, J.L., Frayn, K.N. (1990). Postprandial substrate deposition in human forearm and adipose tissues in vivo. *Clin. Sci. (Lond.)* 79(4): 339-348. doi.org/10.1042/cs0790339

[25] Daly, M.E., Vale, C., Walker, M., Littlefield, A., Alberti, K.G., Mathers, J.C. (1998). Acute effects of insulin sensitivity and diurnal metabolic profiles of a high-sucrose compared with a high-starch diet. *Am. J. Clin. Nutr.* 67(6): 1186-1196.

[26] DeFronzo, R.A., Ferrannini, E. (1982). Influence of plasma glucose and insulin concentration on plasma glucose clearance in man. *Diabetes* 31(8): 683-688. doi.org/10.2337/diab.31.8.683

[27] Deussen, A., Bassingthwaighte, J.B. (1996). Modeling [^{15}O] oxygen tracer data for estimating oxygen consumption. *Am. J. Physiol.* 270(3 Pt 2): H1115-H1130.

[28] Dimitriadis, G., Mitrou, P., Lambadiari, V., Boutati, E., Maratou, E., Koukkou, E., Tzanela, M., Thalassinos, N., Raptis, S.A. (2006). Glucose and lipid fluxes in the adipose tissue after meal ingestion in hyperthyroidism. *J. Clin. Endocrinol. Metab.* 91(3): 1112-1118. doi.org/10.1210/jc.2005-0960

[29] Doege, H., Baillie, R.A., Ortegon, A.M., Tsang, B., Wu, Q., Punreddy, S., Hirsch, D., Watson, N., Gimeno, R., Stahl, A. (2006). Targeted deletion of FATP5 reveals multiple functions in liver metabolism: alterations in hepatic lipid homeostasis. *Gastroenterology* 130: 1245-1258. doi.org/10.1053/j.gastro.2006.02.006

[30] Doege, H., Grimm, D., Falcon, A., Tsang, B., Storm, T.A., Xu, H., Ortegon, A.M., Kazantzis, M., Kay, M.A., Stahl, A. (2008). Silencing of hepatic fatty acid transporter protein 5 *in vivo* reverses diet-induced non-alcoholic fatty liver disease and improves hyperglycemia. *J. Biol. Chem.* 283(32): 22186-22192. doi.org/10.1074/jbc.M803510200

[31] Erdogmus, B., Tamer, A., Buyukkaya, R., Yazici, B., Buyukkaya, A., Korkut, E., Alcelik, A., Korkmaz, U. (2008). Portal vein hemodynamics in patients with non-alcoholic fatty liver disease. *Tohoku J. Exp. Med.* 215(1): 89-93.

[32] Falcon, A., Doege, H., Fluitt, A., Tsang, B., Watson, N., Kay, M.A., Stahl, A. (2010). FATP2 is a hepatic fatty acid transporter and peroxisomal very long-chain acyl-CoA synthetase. *Am. J. Physiol. Endocrinol. Metab.* 299: E384-E393. doi.org/10.1152/ajpendo.00226.2010

[33] Fogler, S. (2001). *Elements of Chemical Reaction Engineering*, 3rd ed. Upper Saddle River, NJ: Prentice Hall.

[34] Forker, E.L., Luxon, B. (1978). Hepatic transport kinetics and plasma disappearance curves: distributed modeling vs. conventional approach. *Am. J. Physiol.* 235: E648-E660.

[35] Fournier, R.L. (1998). *Basic Transport Phenomena in Biomedical Engineering.* New York, NY: Taylor & Francis.

[36] Gebhardt, R. (1992). Metabolic zonation of the liver: regulation and implications for liver function. *Pharmacol. Ther.* 53(3): 275-354.

[37] Gong, Z., Tas, E., Yakar, S., Muzumdar, R. (2017). Hepatic lipid metabolism and non-alcoholic fatty liver disease in aging. *Mol. Cell. Endocrinol.* 455: 115-130. doi.org/10.1016/j.mce.2016.12.022

[38] Gray, M.R., Tam, Y.K. (1987). The series-compartment model for hepatic elimination. *Drug Metab. Dispos.* 15(1): 27-31.

[39] Haas, J.T., Francque, S., Staels, B. (2016). Pathophysiology and mechanisms of nonalcoholic fatty liver disease. *Annu. Rev. Physiol.* 78: 181-205. doi.org/10.1146/annurev-physiol-021115-105331

[40] Hames, K.C., Vella, A., Kemp, B.J., Jensen, M.D. (2014). Free fatty acid uptake in humans with CD36 deficiency. *Diabetes* 63(11): 3606-3614. doi.org/10.2337/db14-0369

[41] Hardy, T., Oakley, F., Anstee, Q.M., Day, C.P. (2016). Nonalcoholic fatty liver disease: pathogenesis and disease spectrum. *Annu. Rev. Pathol. Mech. Dis.* 11: 451-496. doi.org/10.1146/annurev-pathol-012615-044224

[42] Hijmans, B.S., Grefhorst, A., Oosterveer, M.H., Groen, A.K. (2014). Zonation of glucose and fatty acid metabolism in the liver: mechanism and metabolic consequences. *Biochimie* 96: 121-129. doi.org/10.1016/j.biochi.2013.06.007

[43] Hundsdorfer, W., Verwer, J.G. (2003). *Numerical Solution of Time-Dependent Advection-Diffusion-Reaction Equations*. Berlin, Germany: Springer.

[44] Jungermann, K. (1987). Metabolic zonation of liver parenchyma: significance for the regulation of glycogen metabolism, gluconeogenesis, and glycolysis. *Diabetes Metab. Rev.* 3(1): 269-293.

[45] Jungermann, K., Katz, N. (1982). Functional hepatocellular heterogeneity. *Hepatology* 2(3): 385-395.

[46] Jungermann, K., Katz, N. (1989). Functional specialization of different hepatocyte populations. *Physiol. Rev.* 69(3): 708-764.

[47] Jungermann, K., Kietzmann, T. (2000). Oxygen: modulator of metabolic zonation and disease of the liver. *Hepatology* 31(2): 255-260. doi.org/10.1002/hep.510310201

[48] Jungermann, K., Kietzmann, T. (1997). Role of oxygen in the zonation of carbohydrate metabolism and gene expression in liver. *Kidney Int.* 51(2): 402-412.

[49] Jungermann, K., Kietzmann, T. (1996). Zonation of parenchymal and nonparenchymal metabolism in liver. *Annu. Rev. Nutr.* 16: 179-203. doi.org/10.1146/annurev.nu.16.070196.001143

[50] Jungermann, K., Sasse, D. (1978). Heterogeneity of liver parenchymal cells. *Trends Biochem. Sci.* 3(3): P198-P202. doi.org/10.1016/S0968-0004(78)91764-4

[51] Katz, N.R. (1992). Metabolic heterogeneity of hepatocytes across the liver acinus. *J. Nutr.* 122(3 Suppl): 843-849. doi.org/10.1093/jn/122.suppl_3.843

[52] Kietzmann, T. (2017). Metabolic zonation of the liver: the oxygen gradient revisited. *Redox Biol.* 11: 622-630. doi.org/10.1016/j.redox.2017.01.012

[53] Kietzmann, T., Dimova, E.Y., Flúgel, D., Scharf, J.G. (2006). Oxygen: modulator of physiological and pathophysiological processes in the liver. *Z. Gastroenterol.* 44(1): 67-76. doi.org/10.1055/s-2005-858987

[54] Kietzmann, T., Jungermann, K. (1997). Modulation by oxygen of zonal gene expression in liver studied in primary rat hepatocyte cultures. *Cell. Biol. Toxicol.* 13(4-5): 243-255.

[55] Li, Y., Chow, C.C., Courville, A.B., Sumner, A.D., Periwal, V. (2016). Modeling glucose and free fatty acid kinetics in glucose and meal tolerance test. *Theor. Biol. Med. Model.* 13(8). doi.org/10.1186/s12976-016-0036-3

[56] Magalotti, D., Marchesini, G., Ramilli, S., Berzigotti, A., Bianchi, G., Zoli, M. (2004). Splanchnic haemodynamics in non-alcoholic fatty liver disease: effect of a dietary/pharmacological treatment: a pilot study. *Dig. Liver Dis.* 36(6): 406-411. doi.org/10.1016/j.dld.2004.01.023

[57] Mashek, DG. (2013). Hepatic fatty acid trafficking: multiple forks in the road. *Adv. Nut.* 4(6): 697-710.

[58] Miquilena-Colina, M.E., Lima-Cabello, E., Sánchez-Campos, S., García-Mediavilla, M.V., Fernández-Bermejo, M., Lozano-Rodríguez, T., Vargas-Castrillón, J., Buqúe, X., Ochoa, B., Aspichueta, P., González-Gallego, J., García-Monzón, C. (2011). Hepatic fatty acid translocase CD36 upregulation is associated with insulin resistance, hyperinsulinaemia and increased steatosis in non-alcoholic steatohepatitis and chronic hepatitis C. *Gut* 60:1394-1402.

[59] Mitsuyoshi, H., Yasui, K., Harano, Y., Endo, M., Tsuji, K., Minami, M., Itoh, Y., Okanoue, T., Yoshikawa, T. (2009). Analysis of hepatic genes involved in the metabolism of fatty acids and iron in nonalcoholic fatty liver disease. *Hepatol. Res.* 39: 366-373. doi.org/10.1111/j.1872-034X.2008.00464.x

[60] Mohammadi, A., Ghasemi-rad, M., Zahedi, H., Toldi, G., Alinia, T. (2011). Effect of severity of steatosis as assessed ultrasonographically on hepatic vascular indices in non-alcoholic fatty liver disease. *Med. Ultrason.* 13(3): 200-206.

[61] Newberry, E.P., Xie, Y., Kennedy, S., Han, X., Buhman, K.K., Luo, J., Gross, R.W., Davidson, N.O. (2003). Decreased hepatic triglyceride accumulation and altered fatty acid uptake in mice with deletion of the liver fatty acid-binding protein gene. *J. Biol. Chem.* 278(51): 51664-51672.

[62] Ohno, H., Naito, Y., Nakajima, H., Tomita, M. (2008). Construction of a biological tissue model based on a single-cell model: a computer simulation at metabolic heterogeneity in the liver lobule. *Artif. Life* 14(1): 3-28.

[63] Pang, K.S., Weiss, M., Macheras, P. (2007). Advanced pharmacokinetic models based on organ clearance, circulatory, and fractal concepts. *AAPS J.* 9(2): E268-E283.

[64] Park, S., Kim, S.H.J., Ropella, G.E.P., Roberts, M.S., Hunt, C.A. (2010). Tracing multiscale mechanisms of drug disposition in normal and diseased livers. *J. Pharmacol. Exp. Ther.* 334(1): 124-136. doi.org/10.1124/jpet.110.168526

[65] Periwal, V., Chow, C.C., Bergman, R.N., Rick, M., Vega, G.L., Sumner, A.E. (2008). Evaluation of quantitative models of the effect of insulin on lipolysis and glucose disposal. *Am. J. Physiol. Regul. Integr. Comp. Physiol.* 295(4): R1089-R1096. doi.org/10.1152/ajpregu.90426.2008

[66] Probst, I., Schwartz, P., Jungermann, K. (1982). Induction in primary culture of 'gluconeogenic' and 'glycolytic' hepatocytes resembling periportal and perivenous cells. *Eur. J. Biochem.* 126(2): 271-278.

[67] Rajaraman, G., Roberts, M.S., Hung, D., Wang, G.Q., Burczynski, F.J. (2005). Membrane binding proteins are the major determinants for the hepatocellular transmembrane flux of long-chain fatty acids bound to albumin. *Pharm. Res.* 22(11): 1793-1804. doi.org/10.1007/s11095-005-7248-2

[68] Rezania, V., Coombe, D., Tuszynski, J.A. (2016). A physiologically-based flow network model for hepatic drug elimination III: 2D/3D DLA lobule models. *Theor. Biol. Med. Model.* 13(9). doi.org/10.1186/s12976-016-0034-5

[69] Ricken, T., Dahmen, U., Dirsch, O. (2010). A biphasic model for sinusoidal liver perfusion remodeling after outflow obstruction. *Biomech. Model. Mechanobiol.* 9: 435-450. doi.org/10.1007/s10237-009-0186-x

[70] Ricken, T., Werner, D., Holzhütter, H.G., König, M., Dahmen, U., Dirsch, O. (2015). Modeling function-perfusion behavior in liver lobules including tissue, blood, glucose, lactate and glycogen by use of a coupled two-scale PDE-ODE approach. *Biomech. Model. Mechanobiol.* 14: 515-536. doi.org/10.1007/s10237-014-0619-z

[71] Ricken, T., Waschinsky, N., Werner, D. (2018). Simulation of steatosis zonation in liver lobule–a continuummechanical bi-scale, tri-phasic, multi-component approach. In: Wriggers, P., Lenarz, T., eds. *Lecture Notes in Applied and Computational Mechanics*, Vol. 84. Cham, Switzerland: Springer.

[72] Roberts, M.S., Rowland, M. (1986). Correlation between in-vitro microsomal enzyme activity and whole organ hepatic elimination kinetics: analysis with a dispersion model. *J. Pharm. Pharmacol.* 38: 177-181.

[73] Roberts, M.S., Rowland, M. (1985). Hepatic elimination–dispersion model. *J. Pharm. Sci.* 74(5): 585-587. doi.org/10.1002/jps.2600740522

[74] Schleicher, J., Dahmen, U., Guthke, R., Schuster, S. (2017). Zonation of hepatic fat accumulation: insights from mathematical modelling of nutrient gradients and fatty acid uptake. *J. R. Soc. Interface* 14: 20170443. doi.org/10.1098/rsif.2017.0443

[75] Sheikh-Bahaei, S., Maher, J.J., Hunt, C.A. (2010). Computational experiments reveal plausible mechanisms for changing patterns of hepatic zonation of xenobiotic clearance and hepatotoxicity. *J. Theor. Biol.* 265(4): 718-733. doi.org/10.1016/j.jtbi.2010.06.011

[76] Shi, J., Kandror, K.V. (2008). Study of glucose uptake in adipose cells. *Methods Mol. Biol.* 456: 307-315. doi.org/10.1007/978-1-59745-245-8_23

[77] Soresi, M., Giannitrapani, L., Noto, D., Terranova, A., Campagna, M.E., Cefalú, A.B., Giammanco, A., Montalto, G. (2015). Effects of steatosis on hepatic hemodynamics in patients with metabolic syndrome. *Ultrasound Med. Biol.* 41(6): 1545-1552. doi.org/10.1016/j.ultrasmedbio.2015.01.020

[78] Thorburn, A.W., Gumbiner, B., Bulacan, F., Wallace, P., Henry, R.R. (1990). Intracellular glucose oxidation and glycogen synthase activity are reduced in non-insulin-dependent (type II) diabetes independent of impaired glucose uptake. *J. Clin. Invest.* 85(2): 522-529. doi.org/10.1172/JCI114468

[79] Torre, C., Perret, C., Colnot, S. (2010). Molecular determinants of liver zonation. *Prog. Mol. Biol. Transl. Sci.* 97: 127-150. doi.org/10.1016/B978-0-12-385233-5.00005-2

[80] van Ginneken, V., de Vries, E., Verheij, E., van der Greef, J. (2017). Potential biomarkers for "fatty liver" (hepatic steatosis) and hepatocellular carcinoma (HCC) and an explanation of their pathogenesis. *Gastroenterol. Liver Clin. Med.* 1(1): 001.

[81] Wölfle, D., Jungermann, K. (1985). Long-term effects of physiological oxygen concentrations on glycolysis and gluconeogenesis in hepatocyte cultures. *Eur. J. Biochem.* 151(2): 299-303. doi.org/10.1111/j.1432-1033.1985.tb09100.x

[82] Wu, Q., Ortegon, A.M., Tsang, B., Doege, H., Feingold, K.R., Stahl, A. (2006). FATP1 is an insulin-sensitive fatty acid transporter involved in diet-induced obesity. *Mol. Cell. Biol.* 26(9): 3455-3467. doi.org/10.1128/MCB.26.9.3455-3467.2006

[83] Yeh, M.M., Brunt, E.M. (2014). Pathological features of fatty liver disease. *Gastroenterology* 147: 754-764. doi.org/10.1053/j.gastro.2014.07.056